Low-frequency earthquakes observed in close vicinity of repeating earthquakes in the brittle upper crust of Hakodate, Hokkaido, northern Japan

Keisuke Yoshida[1], Akira Hasegawa[1, 2], Shinako Noguchi[2], Keiji Kasahara[2]

1: Research Center for Prediction of Earthquakes and Volcanic Eruptions, Graduate School of Science, Tohoku University

2: Association for the Development of Earthquake Prediction

Corresponding author: Keisuke Yoshida, Research Center for Prediction of Earthquakes and Volcanic Eruptions, Tohoku University, 6-6 Aza-Aoba, Aramaki, Aoba-ku, Sendai, 980-8578, Japan. (keisuke.yoshida.d7@tohoku.ac.jp)

Tel: +81-22-795-6779

Fax: +81-22-264-3292

Abbreviated title: Low-frequency earthquakes near crustal repeating earthquakes

SUMMARY

We conducted a detailed investigation of an earthquake cluster distributed from the lower crust to the upper crust beneath Hakodate, Hokkaido, which included both low-frequency earthquakes (LFEs) and regular earthquakes. Relocated hypocentres clearly show that both the LFEs and regular earthquakes occurred close to each other in the brittle upper crust of this non-volcanic area, while only LFEs occurred in the lower crust. This indicates that LFEs can occur not only in the ductile lower crust, but also in the brittle upper crust, which suggests that LFEs can occur in an environment similar to that of regular earthquakes. Regular earthquakes that occur in close vicinity of LFEs have very similar waveforms and nearly overlapping source regions, which indicate that they reflect the repeated rupture of the same asperity patch on a fault. Temporally, the intervals between events in the repeating earthquake sequence were very short, thus suggesting that they were caused by a sudden increase in pore pressure. The cluster of LFEs and repeating earthquakes, which has a rod-like distribution extending from the bottom of the crust to the surface and tilted slightly eastward, might represent a pathway of aqueous fluid movement sourced from the subducting slab.

Key words: Seismicity and tectonics, Earthquake source observations, Earthquake dynamics, Rheology and friction of fault zones

1. INTRODUCTION

Pore pressure changes at depth affect fault strength and thus play an important role in the generation of earthquakes (e.g. Hubbert & Rubey 1959; Nur & Booker 1972; Rice 1992; Sibson 1992, 2020; Hasegawa 2017). A remarkable example of this is induced seismicity caused by fluid injection (e.g. Healy *et al.* 1968). Fluid injection-induced seismicity has distinct characteristics that are similar to those observed in the swarm activity of natural earthquakes (e.g. Cox 2016), including the seismicity pattern and the migration behaviour of hypocentres (e.g. Shapiro *et al.* 1997; Parotidis *et al*. 2003). Such a similarity suggests that the involvement of fluids also plays an important role in the occurrence of natural earthquakes. This hypothesis is consistent with various geophysical and geological observations of the stress fields, seismic velocity, and attenuation structures (e.g. Sibson 1992, 2020; Hasegawa 2017).

Previous studies have suggested that the occurrence of deep low-frequency earthquakes (LFEs), a special type of earthquake characterized by longer-period seismic waves and greater focal depths (e.g. Ukawa & Ohtake 1987; Hasegawa & Yamamoto 1994; Obara 2002; Katsumata & Kamaya 2003; Rogers & Dragert 2003; Aso *et al*. 2013), is also closely related to fluid behaviour. Deep LFEs can be classified into the following two groups: (1) those occurring in the transition zone between the brittle rupture of a regular earthquake and stable sliding along the plate boundary (e.g. Obara 2002; Katsumata & Kamaya 2003; Rogers & Dragert 2003) and (2) those occurring in the lower crust of the upper plate far from the plate boundary, often located beneath active volcanoes (e.g. Hasegawa & Yamamoto 1994). The first type of deep LFEs are estimated to represent shear faulting along the plate boundary (Ide *et al*. 2007a; Shelly *et al.* 2007), while the generation mechanism of the second type of deep LFEs is not well understood, compared to the former. In fact, deep LFEs of the second type have been estimated to have

significant compensated linear vector dipole (CLVD) components (Nakamichi *et al.* 2003; Aso & Ide 2014). Also, waveforms of the second type of LFEs are characterized by long-lasting high-amplitude codas, which largely differ from those of regular earthquakes and the first type of deep LFEs. This study deals with this second type of deep LFEs. Note that several of these deep LFEs in the lower crust occur away from the plate boundary near volcanoes; however, some are located far from volcanoes (Hasegawa *et al.* 1991, 2005; Hasegawa & Yamamoto 1994; Kamaya & Katsumata 2004; Takahashi & Miyamura 2009). The LFEs that occur near and far from volcanoes have similar features, which suggests that their generation mechanism is very similar (Aso *et al.* 2011, 2013).

The Japan Meteorological Agency (JMA) routinely locates earthquakes that occur in and around the Japanese Islands by using a nationwide seismic network that covers the entire country of Japan. Recent densification of the seismic observation network in the country has considerably improved the earthquake detection capability, and it is now possible to observe in detail the activities of deep LFEs throughout Japan (e.g. Kamaya & Katsumata 2004; Takahashi & Miyamura 2009). Earthquakes that occur in the deep crust and have low frequency components can be distinguished from many other regular earthquakes and are then classified as deep LFEs in the JMA unified earthquake catalogue. Fig. 1(a) shows the lateral distribution of such deep LFEs in northern Japan from January 2003 to October 2018; these data were compiled from the JMA unified catalogue. Many of these events are located at depths near the Mohorovicic discontinuity (30–40 km), which is much deeper than the typical depth limit for regular earthquakes (~10–15 km) and is consequently well below the brittle-ductile transition depth in the mid-crust (Hasegawa & Yamamoto 1994; Omuralieva *et al.* 2012). Previous studies have suggested that the occurrence and characteristics of these deep LFEs are related to deep

82 magmatic activities such as fluid movement (Hasegawa & Yamamoto 1994), fluid-induced
83 oscillations (Aki 1977; Julian 1994), and cooling magma (Aso & Tsai 2014).

84 Most of the deep LFEs classified by the JMA are located at lower crustal depths where
85 regular earthquakes do not occur probably because ductile flow or aseismic slip is the dominant
86 mode of failure. However, exceptions exist in several areas where the events classified as deep
87 LFEs by the JMA are located in the upper crust with similar depths to regular earthquakes
88 (Kosuga and Haruyama 2018; Noguchi *et al*. 2018). A typical example is an area in Hakodate,
89 Hokkaido, in northern Japan (indicated by a green rectangle in Fig. 1b), where many deep LFEs
90 have occurred despite the lack of nearby active volcanoes. Fig. 2 shows the map and cross-
91 sectional views of hypocentres of both regular earthquakes and deep LFEs located by the JMA in
92 this region. The figure indicates that the deep LFEs classified by the JMA are distributed at
93 various crustal depths ranging from 5 to 35 km, which is well above the upper plate boundary of
94 the subducting Pacific plate (at a depth of ~110 km). Shallow LFEs in the upper crust are also
95 located close to shallow regular earthquakes.

96 An important question is what causes the difference between LFEs and regular
97 earthquakes? This study investigated LFEs and regular earthquakes occurring in the
98 aforementioned region of Hakodate, Hokkaido, based on their hypocentre locations and
99 waveform characteristics. The region is covered by a locally dense seismic network (AS-net;
100 Noguchi *et al.* 2017) that has been operated by the Association for the Development of
101 Earthquake Prediction (ADEP) since 2014 (blue inverted triangles in Fig. 1b). Although the
102 accuracy of the relative locations of LFEs from the JMA unified catalogue is not very good,
103 inclusion of the data from this dense local network will contribute to significant improvements in
104 the accuracy of locating the hypocentres of both regular earthquakes and LFEs. This provides a

105 unique opportunity to investigate the relationship between regular earthquakes and LFEs in
106 detail.
107
108 **2. DATA AND METHODS**
109 The distribution of seismic stations used in this study is shown in Fig. 1(b). The stations
110 belong to the AS-net (blue inverted triangles) and the nationwide seismic network in Japan called
111 the Kiban seismic network (black inverted triangles). We relocated the hypocentres of 212
112 earthquakes (M_{JMA} 0.0–2.7) listed in the JMA unified catalogue from this region of Hakodate,
113 Hokkaido, for the period from January 2003 to October 2018 (Fig. 2). Of these earthquakes, 189
114 and 23 were classified as LFEs and regular earthquakes, respectively, in the JMA unified
115 catalogue.
116 For hypocentral relocation, we applied the double-difference location method (Waldhauser
117 & Ellsworth 2000) to the differential arrival time data of P and S waves, following the procedure
118 adopted by Yoshida & Hasegawa (2018a, 2018b). Arrival times for the P and S waves of the
119 target earthquakes at the AS-net stations were manually picked and were used with those listed in
120 the JMA unified catalogue. In addition, we obtained precise differential arrival time data by
121 using waveform cross-correlation, which largely improved the accuracy of relative hypocentre
122 locations. We used waveform data obtained in and around the source region (Fig. 1b), applied a
123 bandpass filter of between 5 and 12 Hz, and computed the cross-correlation function for all event
124 pairs whose horizontal distance was less than 3.0 km. The differential arrival times were adopted
125 if the cross-correlation coefficient was higher than 0.85. We initially measured the timing of the
126 correlation peak to the nearest sample (0.01 s), then refined the timing and height of the peak by
127 performing a simple quadratic interpolation, as in Shelly *et al.* (2016). Durations of 2.5 s and 4.0

s were adopted for P and S wave windows, respectively, starting at 0.3 s before onset. The P wave window was truncated in order to avoid overlapping with the S wave window when S-P times were less than 2.5 s. The assumed seismic velocity structure was the 1-D model proposed in Hasegawa *et al.* (1978), which has been adopted by Tohoku University for routinely determining hypocentre locations and focal mechanisms for events in northeastern Japan. Also, we used another 1-D velocity model, JMA2001, by Ueno *et al.* (2002) to check the robustness of the main results. The velocity models of Hasegawa *et al.* (1978) and Ueno *et al.* (2002) are shown in Fig. S1. Differential arrival time data derived from the manual picking produced 2,459 P wave arrivals and 6,860 S wave arrivals. Waveform cross-correlation delay measurements produced 677 P wave and 643 S wave arrivals.

We evaluated the uncertainty in the hypocentre locations by recalculating the relocations 1000 times based on bootstrap resampling of differential arrival time data. We computed the 95% confidence intervals of longitude, latitude, and focal depth for each earthquake as half the difference of the maximum and minimum values within the 950 solutions close to the main result. The frequency distributions are shown in Fig. S3. The median values of the 95% interval of distances along longitude, latitude, and depth were 1.5 km, 2 km, and 2 km, respectively.

3. RESULTS

Fig. 3 shows the spatial distribution of the relocated hypocentres. Many of the LFEs are clustered in the central region of the study area in a depth range of 15–35 km, dipping slightly eastward. The LFEs are also distributed in the shallow upper crust (~10 km) in the western region, which appears to be a shallow extension of the deeper LFE cluster. The same tendency was obtained for relocated hypocentres based on the velocity model of Ueno *et al.* (2002) (Fig.

S2). Fig. 4 shows examples of the LFE waveforms obtained at the closest Kiban seismic network station (HU.ESH), which is located north of the source region (Fig. 1b) and has been operated by Hokkaido University. The diversity of LFE focal depths can be confirmed by an increasing S-P time with increasing determined focal depth.

Fig. 5 shows an enlarged view of the spatial distribution of regular earthquakes and LFEs in the western region of the study area. The LFEs occurred in the immediate vicinity of regular earthquakes, which is also apparent in the observed waveform records shown in Fig. 6. The S-P times of the regular earthquakes shown in Figs. 6k, l, n, and o are approximately 2.5 s, which are similar to those of LFEs shown in Figs. 6b, c, g, m, r, s, t, x, and A. Moreover, waveforms of the initial phases of direct waves of some LFEs (Figs. 6c, g, and r) are similar to those of the regular earthquakes in Figs. 6k, l, n, and o, thus suggesting that both the propagation- and site-effects of these earthquakes are also similar. These results indicate that LFEs can also occur at depths shallower than the brittle-ductile transition depth (~12 km; Omuralieva *et al.* 2012) and can spatially coexist with regular earthquakes. On the other hand, later phases of the LFEs are characterized by large amplitudes, which are quite different from those of the regular earthquakes.

Key differences between regular earthquakes and LFEs are the dominant frequency and existence or non-existence of long-lasting codas of observed waveforms. From Fig. 6 it is clear that some earthquakes classified as regular earthquakes in the JMA unified catalogue have waveforms with predominantly low frequencies and characteristic high-amplitude later phases (Figs. 6b, m, p, s, t, v, w, x, and B). Waveforms from these earthquakes are very similar to those of events classified as LFEs by the JMA (Figs. 6a, c, d, e, f, g, h, i, j, q, r, u, y, z, A, C, and D). Although classified as regular earthquakes in the JMA catalogue, these events should be

reclassified as LFEs due to the aforementioned characteristics. This indicates that the JMA unified catalogue includes LFEs that have been misclassified as regular earthquakes. Such misclassifications of LFEs in the shallow upper crust are likely because the classifications are routinely made by humans who have prior knowledge that typical LFEs occur deeper than regular earthquakes, well below the brittle-ductile transition depth. In this study, we reclassified the misclassified LFEs in this region. Figs. 5 and 6 show LFEs and regular earthquakes that have been reclassified by manual inspections of their waveforms. Many of the events originally classified as regular earthquakes by the JMA in this region were reclassified as LFEs, and regular earthquakes were actually only a small fraction of the recorded earthquakes in the study area (only four; Figs. 6 k, l, n, and o).

In order to confirm our reclassification of LFEs by manual inspection, we quantitatively assessed the validity of our classification based on the dominant frequency and existence or non-existence of long-lasting codas of observed waveforms. We first computed velocity spectra by applying the multi-taper spectral estimation library of Prieto *et al.* (2009) to the waveforms in Fig. 6, and the results are shown in Fig. 7. We then estimated the dominant frequency of each spectra similarly to the corner frequency of Andrews (1986): $f_d = \frac{1}{2\pi}\sqrt{\frac{\int_{f_1}^{f_2} D^2(f)\,df}{\int_{f_1}^{f_2} V^2(f)\,df}}$, where $D(f)$ and $V(f)$ are the amplitudes of displacement and velocity spectra, respectively. Here, we set f_1 to 2 and f_2 to 20 Hz. We also computed waveform envelopes by using the bandpass-filtered data of

192 waveforms in Fig. 6 for the frequency range of 2–8 Hz in the same way as Hiramatsu *et al.*
193 (2000). We calculated the root mean square (RMS) amplitude in a moving window with a
194 duration of 0.8 s, and the results are shown in Fig. 8. We then determined the decay rate a of the
195 envelope amplitudes by fitting the linear equation $\ln A(t) = at + constant$ by the least squares
196 method using envelopes after the arrival of direct S waves. Here, t is the elapsed time and $A(t)$ is
197 the envelope amplitude. Fig. 9 compares the frequency distributions of the dominant frequency
198 f_d and the decay rate a of regular earthquakes with those of LFEs. We can see two peaks both in
199 the histograms of the dominant frequency (Fig. 9a) and decay rate (Fig. 9b) corresponding to
200 regular earthquakes and LFEs, which supports the validity of our classification. The dominant
201 frequencies of the LFEs are certainly small (~2–5 Hz) compared to the regular earthquakes (~6
202 Hz). The decay rates of the regular earthquakes (< ~-0.5) are different from those of LFEs (-0.3–
203 0.1) as well.

204 Previous studies have suggested that LFEs and regular earthquakes occur at different
205 depths; regular earthquakes occur in the upper crust above the brittle-ductile transition depth,
206 while LFEs occur in the lowermost crust to uppermost mantle, well below the transition depth
207 (e.g. Hasegawa & Yamamoto 1994). Given that regular earthquakes and LFEs occur above and
208 below the brittle-ductile transition depth, respectively, this adds constraints on the potential cause
209 of each type of earthquake, such as the temperature, pressure, and deformation mode. However,
210 the present study shows that some LFEs certainly can occur in almost the same locations as
211 regular earthquakes.

212 The spatial coexistence of regular earthquakes and LFEs suggests that they can occur in
213 similar environments. While LFEs occurred both in the brittle and ductile regions of the crust, as
214 shown in the data, regular earthquakes occurred only in the brittle upper crust. Since active

volcanoes are not located in the study area, the cause of these LFEs is not likely to have been directly related to magmatic activity. One possible explanation is the involvement of non-magmatic fluids. Fluids are also suggested as the cause of regular earthquakes (e.g. Hubbert & Rubey 1959; Nur & Booker 1972; Rice 1992; Sibson 1992; Hasegawa 2017) and deep LFEs along the plate boundary (e.g. Kodaira *et al.* 2004; Shelly *et al.* 2006; Kato *et al.* 2010), in which the effect of increasing pore pressure is thought to play a key role. Increased pore pressure reduces effective normal stress and might affect the rupture speed, slip speed, and stress drop (e.g. Liu & Rice 2005). This also might explain the occurrence of LFEs in the upper crust away from the plate boundary. The rapid movement of fluid and drastic reduction of frictional strength by extremely high pore pressure might enable a fault to slip rapidly by causing a rapid increase in strain rate, even in the ductile lower crust that is governed by the flow law. Fluid flows also may change the anelastic properties around the sources and affect seismic waveforms.

The observed differences between LFEs and regular earthquakes might be due to differences in pore pressure or fluid volume. In fact, seismic waveforms of typical LFEs generally have high S wave amplitudes compared to those of P waves, thus suggesting that shear deformation is also predominant for LFEs. In the ductile part of the crust, effective normal stress must be very small to cause fault-slips (Kohlstedt *et al.* 1995), which might be why only LFEs can occur in the ductile lower crust. Even LFEs are absent at depths greater than 35 km, which might be because the effective normal stress is too small to cause fault-slip rapidly enough to emit observable seismic waves at such depths. However, a reduction in effective normal stress alone cannot explain some characteristics of LFE waveforms, including their significant CLVD components and long-lasting high-amplitude codas. In the present case, regular earthquakes, which do not have the latter feature, occurred near LFEs, which suggests that the long-lasting

codas of LFEs originated at or very close to the sources. This feature is similar to those of volcanic shallow long period (LP) events (e.g. Chouet & Matoza 2013) and some fluid-injection induced events (Bame & Fehler 1986; Ferrazzini *et al.* 1990). These characteristics could be explained by incorporating the effects of the reduction in effective normal stress (decreases in rupture speed, slip speed, and stress drop) with other fluid effects, such as fluid movement (Hasegawa & Yamamoto 1994), nonlinear self-excited oscillations induced by a fluid flow (Julian 1994), or oscillations of fluid-filled resonators (e.g. Kubotera 1974; Aki *et al.* 1977; Chouet 1985), which were proposed to explain the characteristics of volcanic long-period (LP) events.

In Fig. 3, the deep cluster of LFEs in the lower crust dips slightly eastward, and the shallow cluster of LFEs and regular earthquakes in the upper crust seems to be located in the shallow extension of the deeper cluster. Based on precise seismic tomographic images of P and S wave velocity structures in northeastern Japan, Hasegawa and Nakajima (2004) suggested that aqueous fluids that were originally expelled from the subducted Pacific slab are transported through the upwelling flow formed in the mantle wedge and finally reach shallow depths immediately below the Mohorovicic discontinuity of the overriding plate. In fact, according to the results from recent seismic tomography studies, the upwelling flow in the mantle wedge reaches the crust immediately below this region (Zhao *et al.* 2012; Shiina *et al*. 2018). The continuous eastward-dipping zone might represent the pathway of these slab-derived aqueous fluids from the bottom of the lower crust to the shallower region of the upper crust.

4. DISCUSSION

We have shown that LFEs in Hakodate occur even within the upper crust in close vicinity

261 to regular earthquakes. The co-existence of regular earthquakes and LFEs enables us to study the
262 source process of LFEs in more detail. Here, we investigate the characteristics of these spatially
263 co-existing regular earthquakes and LFEs in the upper crust.
264
265 **4.1. Crustal repeating earthquakes due to increased pore pressures**
266 Waveforms of the four regular earthquakes shown in Figs. 6(k), (l), (n), and (o) are very
267 similar, which suggests that these earthquakes occurred at locations very close together. This is
268 supported by the relocated hypocentres shown in Fig. 5. Fig. 10 shows enlarged cross-sectional
269 views of various directions for these four regular earthquakes. We refer to these regular
270 earthquakes as #1, #2, #3, and #4 in Figs. 6 and 10. The size of the circles in the figure
271 corresponds to the circular crack size with a stress drop of 3 MPa, according to Eshelby (1957).
272 The distances between the four regular earthquakes are smaller than their fault sizes, which
273 suggests that they were caused by repeated slip along the same section of a fault. Figs. S4(a)–(f)
274 show the frequency distributions of the distances between the four earthquakes based on the
275 results from 1000 bootstrap re-samplings. In the figures, only 950 results most similar to the
276 main results are displayed to show the 95% confidence region. These figures indicate that
277 distances between the four regular earthquakes are significantly less than 80 m.
278 Fig. 11 shows the waveforms of the two largest events of the four regular earthquakes
279 observed at the nearest seismic station (A.TSRN), which is located northwest of the source
280 region (Fig. 1b). One is an M 1.6 earthquake (event #3 in Figs. 6 and 10) that occurred at 8:02 on
281 6 Dec. 2016 (JST), and the other is an M 1.4 earthquake (event #2) that occurred at 8:13 on 6
282 Dec. 2016 (JST). The time interval between the two events was approximately 10 min. Even the
283 raw waveforms that include both P and S waves are similar (with cross-correlation coefficients

higher than 0.93), thus indicating that their locations are very close together and their focal mechanisms are very similar. If we apply a bandpass filter of 5–12 Hz to the waveforms to remove the effects of rupture process complexity and noise, they become almost identical (with cross-correlation coefficients higher than 0.98).

To confirm the coincidence of source locations of the two earthquakes, we showed the difference in S-P time at each station, i.e. the difference in the differential arrival times of P ($\mathbf{dt_p}$ dt_p) and S waves (dt_s), by using its frequency distribution (Fig. 12a). These values were determined by using the waveform correlation (Section 2), and only those having cross-correlation coefficients higher than 0.95, both for P- and S waves, are shown in the figure. Most of the S-P time differences obtained are concentrated around 0.00 s, with a few exceptions (one sampling deviation). Fig. 12(b) shows the spatial distribution of S-P time differences, in which we do not observe spatial coherence, which suggests that the ~0.01 s deviations come from measurement error of one sampling deviation due to noise. $\mathbf{dt_s - dt_p < 0.03}$ $dt_p - dt_s$<0.003 s at stations in various orientations indicate that the distance between the two events is less than 25 m, assuming the Omori coefficient of 8.3 km/s based on the velocity model in NE Japan (Hasegawa *et al.* 1978). This is much smaller than the source diameter of ~60 m assumed from the stress drop of 3 MPa.

Next, we attempt to estimate fault sizes of these regular earthquakes more directly from corner frequencies of source spectra of S waves. Since the observed waveforms are generally contaminated by the effects of wave propagation, we first need to remove those effects to properly extract information on the earthquake source. We adopted the empirical Green function (EGF) method (Hartzell 1978), in which waveforms of nearby earthquakes are used to remove the propagation effects. When the corner frequency of the numerator event is lower than that of

307 the denominator (EGF) event, the spectral ratios decrease in the frequency range between the
308 lower and the higher corner frequencies. In contrast, the spectral ratio increases when the corner
309 frequency of the numerator event is higher than that of the denominator event. We used time
310 windows with a duration of 5.12 s, starting from 0.3 s before S wave arrival, and computed their
311 amplitude spectra. We also computed the amplitude spectra of noise by using a time window
312 with the same duration but starting from 6 s before P wave arrival. When the signal to noise
313 ratios were higher than 3 for all of the frequency points from 1 to 15 Hz, we computed the ratios
314 between the amplitude spectra of two earthquakes at the same station.

315 Obtained amplitude spectral ratios for the six pairs of the four regular earthquakes are
316 shown by black curves in Fig. 13. The blue curves in the figure show the mean amplitude
317 spectral ratio. The figure shows that the spectral ratios are almost flat for the three pairs (Figs.
318 13a, c, and e) out of the six, thus suggesting that corner frequencies of the M1.6, M1.4, and M0.7
319 events do not exist in the frequency range below ~15 Hz or the corner frequencies of the three
320 events are the same. For the remaining three pairs, spectral ratios are almost flat up to ~8 Hz and
321 then suddenly increase (Figs. 13b and d) or decrease (Fig. 13f) above this frequency. Let us refer
322 to the corner frequencies of the events #1, #2, #3, and #4 as fc_1, fc_2, fc_3, and fc_4, respectively. The
323 spectral ratios increase above ~8 Hz when the spectra of event #2 (Fig. 13b) or event #3 (Fig.
324 13d) are divided by those of event #1. This suggests that fc_1 is smaller than fc_2 and fc_3, and fc_1 is
325 approximately 8 Hz. To be precise, the corner frequency of event #1 obtained according to the
326 method of Andrews (1986) is 7.5 Hz. The spectral ratio decreases above fc_1 when the spectra of
327 event #1 are divided by those of event #4 (Fig. 13f). This suggests that fc_1 (7.5 Hz) is smaller
328 than fc_4.

329 Interestingly, the corner frequency of the M1.1 earthquake (event #1) is smaller than those

of the M1.6 (#2) and M1.4 (#3) earthquakes, thus suggesting that stress drops, rupture speeds, or slip speeds differ among these earthquakes. The source diameter is estimated to be 266 m and the stress drop 0.010 MPa when applying the source model of Sato & Hirasawa (1973) and assuming the value of the rupture velocity divided by the S wave velocity to be 0.9. Here, we estimated the seismic moments by approximating the moment magnitude by the local magnitude (M1.1). The fault size is much larger than the distance between the earthquakes (< 80 m), thus supporting the proposal that these earthquakes are caused by repeating slips at the same asperity patch.

The corner frequency of event #1 is 7.5 Hz, and we did not see the second change of slopes of spectral ratios corresponding to the corner frequencies of the events #2, #3, and #4 in Figs. 13 (b), (d), and (f). These observations suggest that their corner frequencies are out of the frequency range (> ~15 Hz), which denotes that the fault diameters of the three earthquakes are less than ~130 m.

Many repeating earthquakes have been observed along plate boundary faults (e.g. Nadeau *et al.* 1995; Igarashi *et al.* 2001; Matsuzawa *et al.* 2002; Uchida *et al.* 2003; Kimura *et al.* 2006). Earthquakes in each repeating earthquake sequence occur at approximately regular intervals and are interpreted as repeated slip on the same asperity patch of the plate interface that is caused by the loading of aseismic slip in the surrounding stable sliding area. On the other hand, recent fluid-injection experiments have shown that repeating earthquakes also occur along crustal faults that are not plate boundaries (Bourouis & Bernard 2007; Lengliné *et al.* 2014; Lin *et al.* 2016). In this case, events in the same repeating earthquake sequence occur over short time intervals. These events are thought to be caused by drastic increases in pore pressure due to fluid-injection and/or the loading of the surrounding creep caused by increased pore pressure.

The results of the present study suggest that natural repeating earthquakes also can occur

because of increases in pore pressure, similar to fluid-injection induced seismicity. The repeating earthquakes observed near the LFEs in Hakodate took place over a very short time interval of approximately 10 min. Similar repeating earthquake occurrences over such a short time interval have also been observed in the induced seismicity of a recent fluid-injection experiment (Lengliné *et al.* 2014). Loading due to aseismic slip in the surrounding stable sliding area seems to be less likely to have caused earthquake recurrence over such a short time interval. Rather, the earthquakes might have been caused by successive reductions in fault strength driven by drastic pore pressure increases. Previous studies suggest that the earthquake stress drop decreases with increasing pore pressure (Allmann & Shearer 2007; Chen & Shearer 2011; Goertz-Allmann *et al.* 2011; Yoshida *et al.* 2017). The extremely small stress drop observed for the M1.1 earthquake might have been due to very high pore pressures during this period.

4.2. Source properties of LFEs

The difference in the frequency component between LFEs and regular earthquakes is essential for understanding the LFE generation mechanism. There are currently questions regarding the spectral characteristics of LFEs that occur along the plate boundary (Ide *et al.* 2007b; Zhang *et al.* 2011). Source displacement spectral amplitudes of regular earthquakes are known to decrease with the square of frequency above the corner frequency, but those of LFEs might be different. In fact, previous studies suggest that LFEs along the plate boundary have a smaller displacement amplitude decay rate with frequency (Ide *et al.* 2007b; Shelly *et al.* 2007), which can be explained by a source time function similar to a boxcar. On the other hand, Zhang *et al.* (2011) analysed non-volcanic tremors in Cascadia and concluded that their spectral falloff is similar to that of regular earthquakes. In this case, the main difference between regular

earthquakes and LFEs results only from the source corner frequency rather than the spectral falloff. To address spectral differences, we investigated the source spectra of the LFEs in Hakodate that occurred in the vicinity of the regular earthquakes. In the present study, we can use waveforms of these nearby high-frequency regular earthquakes as EGFs.

We used the earthquake pair from the largest regular earthquake (M 1.6) (Fig. 6n, #3) and a nearby LFE of M 0.9 (Fig. 6r, L1), for which waveform data from AS-net (operated since 2014) were available. The two hypocentres are very close together, and their initial parts of the P wave (< ~0.3s) have similar waveforms, thus suggesting that their propagation effects can be removed by using the EGF method. We computed the velocity spectra of the observed waveforms by using time windows with a duration of 5.12 s, starting from 0.3 s before the S wave arrival and computed their amplitude spectra (red and blue curves in Fig. 14a). We also computed the amplitude spectra of noise by using a time window with the same duration but starting from 6 s before the P wave arrival (green curves in Fig. 14a). When the signal to noise ratios were higher than 3 for all of the frequency points from 1 to 15 Hz, we computed the ratios between the amplitude spectra of two earthquakes at the same station, shown by black curves in Fig. 14(b). The red curve in Fig. 14(b) shows the mean amplitude spectral ratio.

Because the corner frequency of the regular earthquake is higher than 15 Hz, the obtained spectral ratios basically reflect the shape of the LFE source spectra. The spectral ratio roughly decays linearly with the frequency, which is different from the omega-square characteristics (Aki 1967) of regular earthquakes in the frequency range from the corner frequency of ~2 Hz to the analysed upper limit of ~15 Hz. This suggests that the difference in the frequency components of LFEs and regular earthquakes results from not only the corner frequency but also the decay rate above the corner frequency, as suggested for the plate boundary LFEs in Japan (Ide *et al.* 2007b;

399 Shelly *et al.* 2007).

400 We also examined other LFEs (L2, L3, L4, and L5 in Fig. 6) that occurred in close vicinity
401 of the M1.6 regular earthquake. Figs. 15(b), (c), (d), (e), and (f) show the obtained spectral ratios
402 of M0.9. M0.6, M0.8, M0.7, and M0.3 LFEs, respectively, with the M1.6 regular earthquake. We
403 only used LFEs that occurred after the installation of the AS-net. Their locations are shown in
404 Fig. 5. The distances of these LFEs from the M1.6 regular earthquakes are less than 2 km (Figs.
405 S4g–k). Fig. 15(a) shows the average of these spectral ratios. The decay rates in these cases of
406 other LFEs also follow the inverse of frequency similar to the case of Fig. 14, thus suggesting
407 that the style of the temporal evolution of moment release is generally different between regular
408 earthquakes and LFEs.

409 Although the local magnitude of the M 0.9 LFE in Fig. 14 is smaller than that of the
410 regular earthquake (M 1.6), the amplitude ratio is almost one in the low frequency range of 1–2
411 Hz, thus indicating that their seismic moments are almost the same. The LFEs have much lower
412 corner frequencies (~2 Hz) than the regular earthquake with a similar seismic moment, which
413 suggests that the stress drop is extremely low or that the rupture and/or slip speed is quite small.

414 The difference in corner frequency cannot explain all of the features of typical LFEs,
415 including non-DC components (e.g. Ukawa & Ohtake 1987; Nishidomi & Takeo 1996; Okada &
416 Hasegawa 2000; Ohmi & Obara 2002; Nakamichi *et al.* 2003; Aso & Ide 2014) and long-lasting
417 high-amplitude characteristic codas. The existence of long-lasting codas is similar to the
418 characteristics of some earthquakes induced by fluid-injection (Bame & Fehler 1986; Ferrazzini
419 *et al.* 1990) and volcanic LP events (e.g. Chouet & Matoza 2013). Explaining these features of
420 the LFEs probably will require a more complicated mechanism, in which some other process
421 such as fluid movement (Hasegawa & Yamamoto 1994) or flow-induced oscillations (Aki *et al.*

422 1977; Chouet 1981; Julian 1994) is combined with shear faulting.

423

424 **5. CONCLUSIONS**

425 We investigated the relationship between regular earthquakes and LFEs in a seismic
426 cluster that extends from the bottom of the crust to the surface, beneath Hakodate, Hokkaido. A
427 dense local seismic network covering this region made it possible to investigate this relationship
428 in detail. Relocated hypocentres and observed waveforms clearly show that both regular
429 earthquakes and LFEs occur in close proximity to each other in the brittle upper crust, although
430 only LFEs occur in the ductile lower crust. This indicates that LFEs can not only occur in the
431 ductile part of the crust, but also in the brittle part of the shallow crust, thus suggesting that the
432 environments causing regular earthquakes and LFEs can be similar. The deep cluster of
433 earthquakes, composed of LFEs, in the lower crust seems to connect with a shallower cluster of
434 earthquakes composed of both LFEs and regular earthquakes. As a whole, the earthquakes have a
435 rod-like distribution extending from the bottom of the crust to near the surface and dipping
436 slightly eastward. This continuous eastward-dipping zone that extends through the entire crust
437 might represent a pathway of aqueous fluids originally sourced from the subducting slab.

438 Regular earthquakes that occur in the close vicinity of LFEs in the upper crust have very
439 similar waveforms, and the separations between their relocated hypocentres are sufficiently
440 smaller than their source diameters. This indicates that these regular earthquakes are repeated
441 ruptures of the same asperity patch. Similar crustal repeating earthquakes have been reported in
442 induced seismicity by fluid-injection experiments (Bourouis & Bernard 2007; Lengliné *et al.*
443 2014). The similarity and co-location with LFEs supports the proposal that these repeating
444 earthquakes were caused by drastic increases in pore pressure.

Inspection of the observed earthquake waveforms has shown that some LFEs that occur in the shallow upper crust were originally misclassified as regular earthquakes in the JMA unified catalogue. This suggests that more LFEs exist in the shallow upper crust than are presently listed in the JMA unified catalogue, which might be an important clue to understanding their generation mechanism.

ACKNOWLEDGMENTS

We deeply thank the editor Professor Ni and two anonymous reviewers for their constructive comments, which helped to improve the manuscript. We used waveform data from the seismic stations of the National Research Institute for Earth Science and Disaster Resilience (NIED), Hokkaido University, Hirosaki University, Tohoku University, the Japan Meteorological Agency (JMA), and the Association for the Development of Earthquake Prevention (ADEP). The figures in this paper were created by using Generic Mapping Tools (GMT) (Wessel & Smith 1998). The data used in this paper are available by contacting the corresponding author at keisuke.yoshida.d7@tohoku.ac.jp.

21

REFERENCES

Aki, K. (1967) Scaling law of seismic spectrum. J. Geophys. Res., 72, 1217–1231, Wiley Online Library.

Aki, K., Fehler, M. & Das, S. (1977) Source mechanism of volcanic tremor: Fluid-driven crack models and their application to the 1963 Kilauea eruption. J. Volcanol. Geotherm. Res., 2, 259–287, Elsevier.

Allmann, B.P. & Shearer, P.M. (2007) Spatial and temporal stress drop variations in small earthquakes near Parkfield, California. J. Geophys. Res. Solid Earth, 112, 1–17. doi:10.1029/2006JB004395

Andrews, D.J. (1986) Objective determination of source parameters and similarity of earthquakes of different size. Earthq. source Mech., 37, 259–267, Wiley Online Library.

Aso, N. & Ide, S. (2014) Focal mechanisms of deep low-frequency earthquakes in Eastern Shimane in Western Japan. J. Geophys. Res. Solid Earth, 119, 364–377, Wiley Online Library.

Aso, N., Ohta, K. & Ide, S. (2011) Volcanic-like low-frequency earthquakes beneath Osaka Bay in the absence of a volcano. Geophys. Res. Lett., 38, Wiley Online Library.

Aso, N., Ohta, K. & Ide, S. (2013) Tectonic, volcanic, and semi-volcanic deep low-frequency earthquakes in western Japan. Tectonophysics, 600, 27–40, Elsevier.

Aso, N. & Tsai, V.C. (2014) Cooling magma model for deep volcanic long-period earthquakes. J. Geophys. Res. Solid Earth, 119, 8442–8456, Wiley Online Library.

Bame, D. & Fehler, M. (1986) Observations of long period earthquakes accompanying hydraulic fracturing. Geophys. Res. Lett., 13, 149–152, Wiley Online Library.

Bourouis, S. & Bernard, P. (2007) Evidence for coupled seismic and aseismic fault slip during water injection in the geothermal site of Soultz (France), and implications for seismogenic transients. Geophys. J. Int., 169, 723–732, Blackwell Publishing Ltd Oxford, UK.

Chen, X. & Shearer, P.M. (2011) Comprehensive analysis of earthquake source spectra and swarms in the Salton Trough, California. J. Geophys. Res. Solid Earth, 116, 1–17. doi:10.1029/2011JB008263

Chouet, B. (1981) Ground motion in the near field of a fluid-driven crack and its interpretation in the study of shallow volcanic tremor. J. Geophys. Res. Solid Earth, 86, 5985–6016, Wiley Online Library.

Chouet, B. (1985) Excitation of a buried magmatic pipe: a seismic source model for volcanic tremor. J. Geophys. Res. Solid Earth, 90, 1881–1893, Wiley Online Library.

Chouet, B. (1986) Dynamics of a fluid-driven crack in three dimensions by the finite difference method. J. Geophys. Res. Solid Earth, 91, 13967–13992, Wiley Online Library.

Chouet, B.A. & Matoza, R.S. (2013) A multi-decadal view of seismic methods for detecting precursors of magma movement and eruption. J. Volcanol. Geotherm. Res., 252, 108–175, Elsevier.

Cox, S.F. (2016) Injection-driven swarm seismicity and permeability enhancement: Implications for the dynamics of hydrothermal ore systems in high fluid-flux, overpressured faulting regimes—An invited paper. Econ. Geol., 111, 559–587, Society of Economic Geologists.

Eshelby, J.D. (1957) The determination of the elastic field of an ellipsoidal inclusion, and related problems. Proc. R. Soc. London. Ser. A. Math. Phys. Sci., 241, 376–396, The Royal Society London.

505 Ferrazzini, V., Chouet, B., Fehler, M. & Aki, K. (1990) Quantitative analysis of long-period
506 events recorded during hydrofracture experiments at Fenton Hill, New Mexico. J.
507 Geophys. Res. Solid Earth, 95, 21871–21884, Wiley Online Library.
508 Goertz-Allmann, B.P., Goertz, A. & Wiemer, S. (2011) Stress drop variations of induced
509 earthquakes at the Basel geothermal site. Geophys. Res. Lett., 38, n/a-n/a.
510 doi:10.1029/2011GL047498
511 Hartzell, S.H. (1978) Earthquake aftershocks as Green's functions. Geophys. Res. Lett.
512 doi:10.1029/GL005i001p00001
513 Hasegawa, A. (2017) Role of H2O in Generating Subduction Zone Earthquakes. Monogr.
514 Environ. Earth Planets, 5, 1–34. doi:10.5047/meep.2017.00501.0001
515 Hasegawa, A. & Nakajima, J. (2004) Geophysical constraints on slab subduction and arc
516 magmatism. State Planet Front. Challenges Geophys., 150, 81–93, Wiley Online Library.
517 Hasegawa, A., Umino, N. & Takagi, A. (1978) Double-planed structure of the deep seismic zone
518 in the northeastern Japan arc. Tectonophysics, 47, 43–58. doi:10.1016/0040-
519 1951(78)90150-6
520 Hasegawa, A. & Yamamoto, A. (1994) Deep, low-frequency microearthquakes in or around
521 seismic low-velocity zones beneath active volcanoes in northeastern Japan.
522 Tectonophysics, 233, 233–252, Elsevier.
523 Hasegawa, A., Zhao, D., Hori, S., Yamamoto, A. & Horiuchi, S. (1991) Deep structure of the
524 northeastern Japan arc and its relationship to seismic and volcanic activity. Nature, 352,
525 683, Nature Publishing Group.

526 Hasegawa, A., Nakajima, J., Umino, N. & Miura, S. (2005) Deep structure of the northeastern
527 Japan arc and its implications for crustal deformation and shallow seismic activity.
528 Tectonophysics, 403, 59–75. doi:10.1016/j.tecto.2005.03.018
529 Healy, J.H., Rubey, W.W., Griggs, D.T. & Raleigh, C.B. (1968) The Denver earthquakes. Science
530 (80-.)., 161, 1301–1310.
531 Hiramatsu, Y., Hayashi, N., Furumoto, M. & Katao, H. (2000) Temporal changes in coda Q- 1
532 and b value due to the static stress change associated with the 1995 Hyogo-ken Nanbu
533 earthquake. J. Geophys. Res. Solid Earth, 105, 6141–6151, Wiley Online Library.
534 Hubbert, M.K. & Rubey, W.W. (1959) Role of fluid overpressure in the mechanics of overthrust
535 faulting. Geol. Soc. Am. Bull., 70, 167–206. doi:10.1130/0016-7606(1959)70
536 Ide, S., Shelly, D.R. & Beroza, G.C. (2007a) Mechanism of deep low frequency earthquakes:
537 Further evidence that deep non-volcanic tremor is generated by shear slip on the plate
538 interface. Geophys. Res. Lett., 34. doi:10.1029/2006GL028890
539 Ide, S., Beroza, G.C., Shelly, D.R. & Uchide, T. (2007b) A scaling law for slow earthquakes.
540 Nature, 447, 76–79. doi:10.1038/nature05780
541 Igarashi, T., Matsuzawa, T., Umino, N. & Hasegawa, A. (2001) Spatial distribution of focal
542 mechanisms for interplate and intraplate earthquakes associated with the subducting
543 Pacific plate beneath the northeastern Japan arc: A triple-planed deep seismic zone. J.
544 Geophys. Res. Solid Earth, 106, 2177–2191, Wiley Online Library.
545 Julian, B.R. (1994) Volcanic tremor: nonlinear excitation by fluid flow. J. Geophys. Res. Solid
546 Earth, 99, 11859–11877, Wiley Online Library.

Kato, A., Iidaka, T., Ikuta, R., Yoshida, Y., Katsumata, K., Iwasaki, T., Sakai, S., et al. (2010) Variations of fluid pressure within the subducting oceanic crust and slow earthquakes. Geophys. Res. Lett., 37, Wiley Online Library.

Kamaya, N. & Katsumata, A. (2004) Low-frequency events away from volcanoes in the Japan Islands. Zishin, 57, 11–28.

Katsumata, A. & Kamaya, N. (2003) Low-frequency continuous tremor around the Moho discontinuity away from volcanoes in the southwest Japan. Geophys. Res. Lett., 30, 20–21, Wiley Online Library.

Kimura, H., Kasahara, K., Igarashi, T. & Hirata, N. (2006) Repeating earthquake activities associated with the Philippine Sea plate subduction in the Kanto district, central Japan: A new plate configuration revealed by interplate aseismic slips. Tectonophysics, 417, 101–118, Elsevier.

Kodaira, S., Iidaka, T., Kato, A., Park, J.-O., Iwasaki, T. & Kaneda, Y. (2004) High pore fluid pressure may cause silent slip in the Nankai Trough. Science (80-.)., 304, 1295–1298, American Association for the Advancement of Science.

Kohlstedt, D.L., Evans, B. & Mackwell, S.J. (1995) Strength of the lithosphere: Constraints imposed by laboratory experiments. J. Geophys. Res. Solid Earth, 100, 17587–17602, Wiley Online Library.

Kosuga, M. & Haruyama, T. (2018) Spectral characteristics of waveforms of deep low-frequency microearthquakes beneath northeastern Japan. Prog. Abst. Seism. Soc. Japan.

Kubotera, A. (1974) Volcanic tremors at Aso volcano. in Developments in Solid Earth Geophysics, Vol. 6, pp. 29–47, Elsevier.

569 Lengliné, O., Lamourette, L., Vivin, L., Cuenot, N. & Schmittbuhl, J. (2014) Fluid-induced
570 earthquakes with variable stress drop. J. Geophys. Res. Solid Earth, 119, 8900–8913,
571 Wiley Online Library.
572 Lin, Y.Y., Ma, K.F., Kanamori, H., Alex Song, T.R., Lapusta, N. & Tsai, V.C. (2016) Evidence
573 for non-self-similarity of microearthquakes recorded at a Taiwan borehole seismometer
574 array. Geophys. J. Int., 206, 757–773. doi:10.1093/gji/ggw172
575 Liu, Y. & Rice, J.R. (2005) Aseismic slip transients emerge spontaneously in three-dimensional
576 rate and state modeling of subduction earthquake sequences. J. Geophys. Res. Solid Earth,
577 110, Wiley Online Library.
578 Matsuzawa, T., Igarashi, T. & Hasegawa, A. (2002) Characteristic small-earthquake sequence off
579 Sanriku, northeastern Honshu, Japan. Geophys. Res. Lett., 29, 38, Wiley Online Library.
580 Nadeau, R.M., Foxall, W. & McEvilly, T. V. (1995) Clustering and periodic recurrence of
581 microearthquakes on the San Andreas fault at Parkfield, California. Science (80-.)., 267,
582 503–507, American Association for the Advancement of Science.
583 Nakajima, J., Hirose, F. & Hasegawa, A. (2009) Seismotectonics beneath the tokyo metropolitan
584 area, Japan: Effect of slab-slab contact and overlap on seismicity. J. Geophys. Res. Solid
585 Earth, 114, 1–23. doi:10.1029/2008JB006101
586 Nakamichi, H., Hamaguchi, H., Tanaka, S., Ueki, S., Nishimura, T. & Hasegawa, A. (2003)
587 Source mechanisms of deep and intermediate-depth low-frequency earthquakes beneath
588 Iwate volcano, northeastern Japan. Geophys. J. Int., 154, 811–828, Blackwell Publishing
589 Ltd Oxford, UK.
590 Nishidomi, I. & Takeo, M. (1996) Seismicity and a focal mechanism of low-frequency
591 earthquakes occurring in the western part of Tochigi prefecture, Japan. Kazan, 41, 43–59.

592 Noguchi, S., Sekine, S., Sawada, Y., Kasahara, K., Sasaki, S., Tazawa, Y. & Yajima, H. (2017)
593 Earthquake monitoring using dense local seismic network, AS-net, in northern Tohoku,
594 Japan. 16th WCEE, Santiago.
595 Noguchi, S., Sekine, S., Sawada, Y., Kasahara, K., Sasaki, S., Y., T., Yajima, H., et al. (2018)
596 Distribution and characteristics of low frequency events observed by AS-net at northern
597 Tohoku and southwestern Hokkaido. Prog. Abst. Seism. Soc. Japan, S23-P26.
598 Nur, A. & Booker, J.R. (1972) Aftershocks caused by pore fluid flow? Science (80-.)., 175, 885–
599 887. doi:10.1126/science.175.4024.885
600 Obara, K. (2002) Nonvolcanic deep tremor associated with subduction in southwest Japan.
601 Science (80-.)., 296, 1679–1681, American Association for the Advancement of Science.
602 Ohmi, S. & Obara, K. (2002) Deep low-frequency earthquakes beneath the focal region of the
603 Mw 6.7 2000 Western Tottori earthquake. Geophys. Res. Lett., 29, 51–54, Wiley Online
604 Library.
605 Okada, T. & Hasegawa, A. (2000) Activity of deep low-frequency microearthquakes and their
606 moment tensors in northeastern Japan. Bull. Volcan. Soc. Jap., 45, 47–63.
607 Omuralieva, A.M., Hasegawa, A., Matsuzawa, T., Nakajima, J. & Okada, T. (2012) Lateral
608 variation of the cutoff depth of shallow earthquakes beneath the Japan Islands and its
609 implications for seismogenesis. Tectonophysics, 518–521, 93–105, Elsevier B.V.
610 doi:10.1016/j.tecto.2011.11.013
611 Parotidis, M., Rothert, E. & Shapiro, S.A. (2003) Pore-pressure diffusion: A possible triggering
612 mechanism for the earthquake swarms 2000 in Vogtland/NW-Bohemia, central Europe.
613 Geophys. Res. Lett., 30, n/a-n/a. doi:10.1029/2003GL018110

614 Prieto, G.A., Parker, R.L. & Vernon, F.L. (2009) A Fortran 90 library for multitaper spectrum
615 analysis. Comput. Geosci., 35, 1701–1710. doi:10.1016/j.cageo.2008.06.007
616 Rice, J.R. (1992) Fault stress states, pore pressure distributions, and the weakness of the San
617 Andreas fault. in International geophysics, Vol. 51, pp. 475–503, Elsevier.
618 Rogers, G. & Dragert, H. (2003) Episodic tremor and slip on the Cascadia subduction zone: The
619 chatter of silent slip. Science (80-.)., 300, 1942–1943, American Association for the
620 Advancement of Science.
621 Sato, T. & Hirasawa, T. (1973) Body wave spectra from propagating shear cracks. J. Phys. Earth,
622 21, 415–431. doi:10.4294/jpe1952.21.415
623 Shapiro, S.A., Huenges, E. & Borm, G. (1997) Estimating the crust permeability from fluid-
624 injection-induced seismic emission at the KTB site. Geophys. J. Int., 131.
625 doi:10.1111/j.1365-246X.1997.tb01215.x
626 Shelly, D.R., Beroza, G.C. & Ide, S. (2007) Non-volcanic tremor and low-frequency earthquake
627 swarms. Nature, 446, 305–307. doi:10.1038/nature05666
628 Shelly, D.R., Beroza, G.C., Ide, S. & Nakamula, S. (2006) Low-frequency earthquakes in
629 Shikoku, Japan, and their relationship to episodic tremor and slip. Nature, 442, 188–191.
630 doi:10.1038/nature04931
631 Shelly, D.R., Ellsworth, W.L. & Hill, D.P. (2016) Fluid-faulting evolution in high definition:
632 Connecting fault structure and frequency-magnitude variations during the 2014 Long
633 Valley Caldera, California, earthquake swarm. J. Geophys. Res. Solid Earth, 121, 1776–
634 1795. doi:10.1002/2015JB012719.Received
635 Shiina, T., Takahashi, H., Okada, T. & Matsuzawa, T. (2018) Implications of Seismic Velocity
636 Structure at the Junction of Kuril-Northeastern Japan Arcs on Active Shallow Seismicity

637 and Deep Low-Frequency Earthquakes. J. Geophys. Res. Solid Earth, 123, 8732-8747,
638 Wiley Online Library.
639 Sibson, R.H. (1992) Implications of fault-valve behaviour for rupture nucleation and recurrence.
640 Tectonophysics, 211, 283–293. doi:10.1016/0040-1951(92)90065-E
641 Sibson, R.H. (2020) Preparation zones for large crustal earthquakes consequent on fault-valve
642 action. Earth, Planets Sp., 72, 1–20, Springer.
643 Takahashi, H. & Miyamura, J. (2009) Deep low-frequency earthquakes occurring in Japanese
644 Islands. Geophys Bull Hokkaido Univ, 72, 177–190.
645 Uchida, N., Matsuzawa, T., Hasegawa, A. & Igarashi, T. (2003) Interplate quasi-static slip off
646 Sanriku, NE Japan, estimated from repeating earthquakes. Geophys. Res. Lett., 30, Wiley
647 Online Library.
648 Ueno, H., Hatakeyama, S., Aketagawa, T., Funasaki, J. & Hamada, N. (2002) Improvement of
649 hypocenter determination procedures in the Japan Meteorological Agency. Q. J. Seism.,
650 65, 123–134.
651 Ukawa, M. & Ohtake, M. (1987) A monochromatic earthquake suggesting deep-seated magmatic
652 activity beneath the Izu-Ooshima Volcano, Japan. J. Geophys. Res. Solid Earth, 92,
653 12649–12663, Wiley Online Library.
654 Waldhauser, F. & Ellsworth, W.L. (2000) A Double-difference Earthquake location algorithm:
655 Method and application to the Northern Hayward Fault, California. Bull. Seismol. Soc.
656 Am., 90, 1353–1368. doi:10.1785/0120000006
657 Wessel, P. & Smith, W.H.F. (1998) New, improved version of generic mapping tools released.
658 Eos, Trans. Am. Geophys. Union, 79, 579–579. doi:10.1029/98EO00426

Yoshida, K., Saito, T., Urata, Y., Asano, Y. & Hasegawa, A. (2017) Temporal Changes in Stress Drop, Frictional Strength, and Earthquake Size Distribution in the 2011 Yamagata-Fukushima, NE Japan, Earthquake Swarm, Caused by Fluid Migration. J. Geophys. Res. Solid Earth, 122, 10,379-10,397. doi:10.1002/2017JB014334

Yoshida, K. & Hasegawa, A. (2018a) Hypocenter Migration and Seismicity Pattern Change in the Yamagata-Fukushima Border, NE Japan, Caused by Fluid Movement and Pore Pressure Variation. J. Geophys. Res. Solid Earth, 123, 5000–5017. doi:10.1029/2018JB015468

Yoshida, K. & Hasegawa, A. (2018b) Sendai-Okura earthquake swarm induced by the 2011 Tohoku-Oki earthquake in the stress shadow of NE Japan: Detailed fault structure and hypocenter migration. Tectonophysics, 733, 132–147, Elsevier. doi:10.1016/j.tecto.2017.12.031

Zhang, J., Gerstoft, P., Shearer, P.M., Yao, H., Vidale, J.E., Houston, H. & Ghosh, A. (2011) Cascadia tremor spectra: Low corner frequencies and earthquake-like high-frequency falloff. Geochemistry, Geophys. Geosystems, 12, Wiley Online Library.

Zhao, D., Yanada, T., Hasegawa, A., Umino, N. & Wei, W. (2012) Imaging the subducting slabs and mantle upwelling under the Japan Islands. Geophys. J. Int., 190, 816–828, Blackwell Publishing Ltd Oxford, UK.

Figures

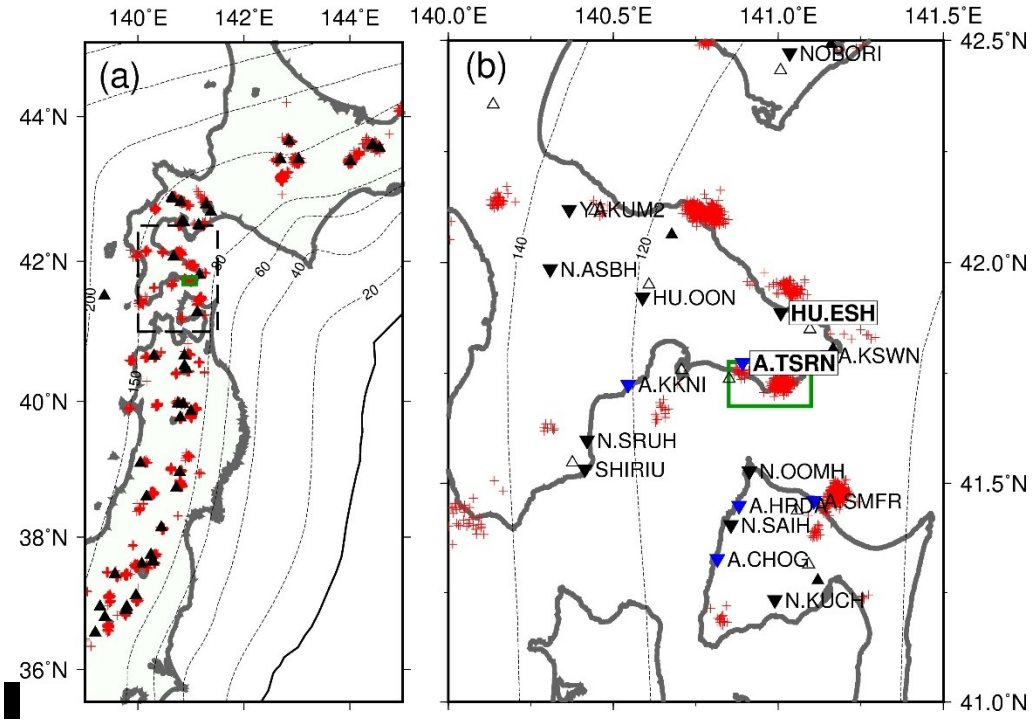

Figure 1. Epicentre distributions of deep LFEs for the period from January 2003 to October 2018 (a) in northern Japan and (b) in the region shown by a dashed rectangle in (a). Red crosses indicate the epicentres of the deep LFEs and black triangles indicate active volcanoes. Open triangles and inverted triangles in (b) indicate Quaternary volcanoes, and seismic stations, respectively. Blue inverted triangles in (b) indicate stations operated by the Association for the Development of Earthquake Prediction (ADEP). The green rectangle in (b) indicates the area of interest in this study. Dotted contours show the depth to the upper plate interface of the subducting Pacific plate (data from Nakajima *et al.* 2009).

32

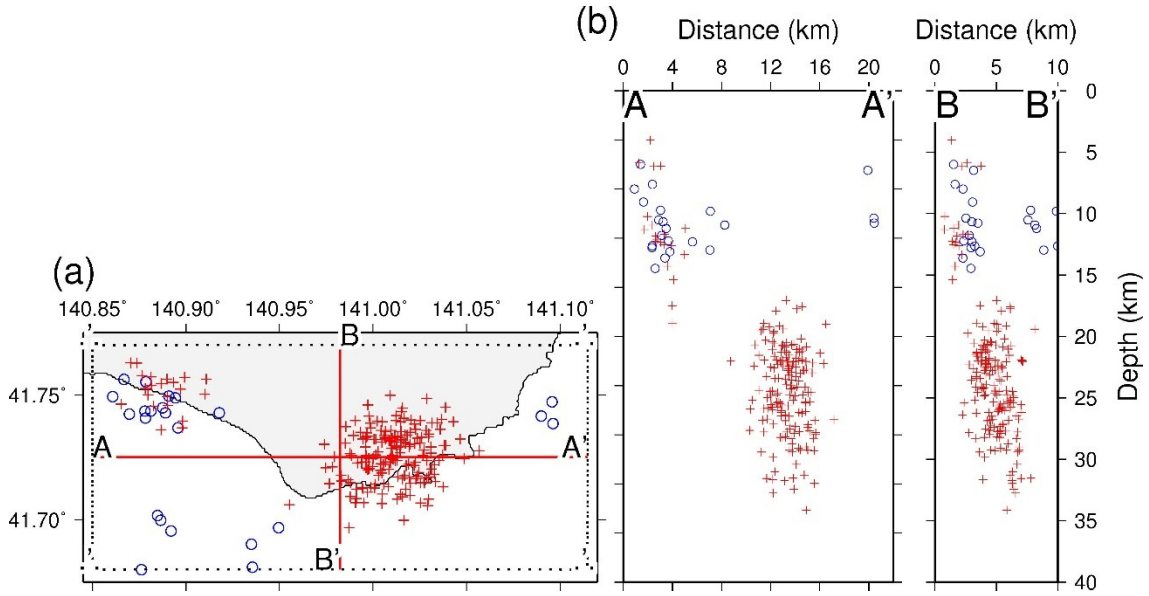

Figure 2. Hypocentres of regular earthquakes and LFEs in Hakodate, Hokkaido, from the JMA unified catalogue for the period from January 2003 to October 2018. (a) Map view. (b) Cross-sectional views along lines A-A' and B-B' in (a). Blue circles and red crosses show the hypocentres of regular earthquakes and LFEs, respectively.

33

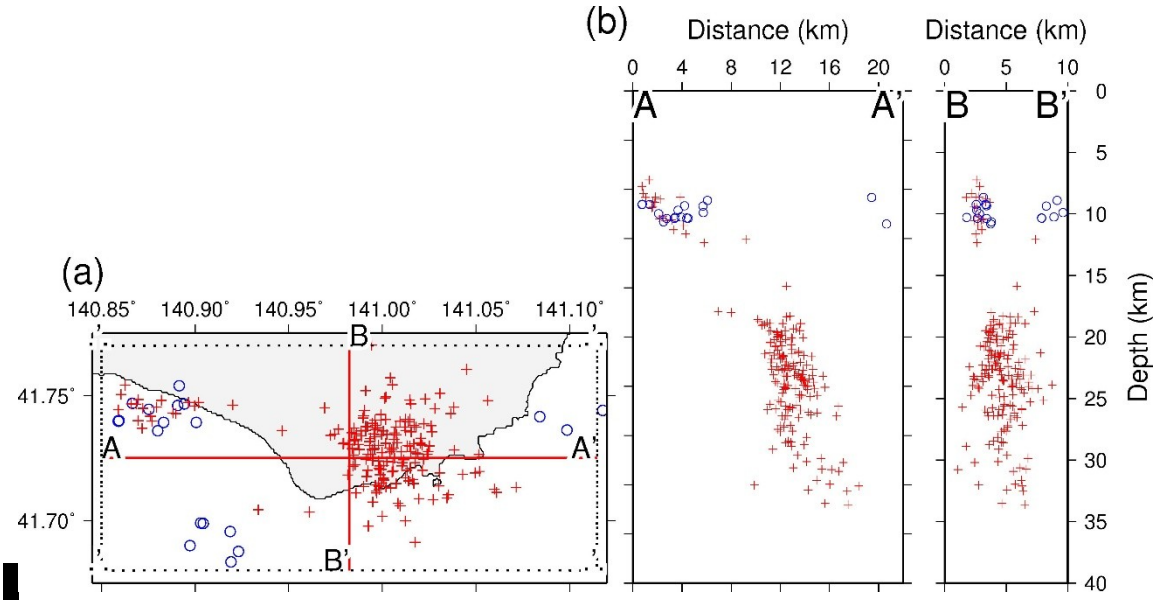

Figure 3. Relocated hypocentres of regular earthquakes and LFEs in Hakodate, Hokkaido. (a) Map view. (b) Cross-sectional views along lines A-A' and B-B' in (a). Blue circles and red crosses show hypocentres of regular earthquakes and LFEs, respectively.

34

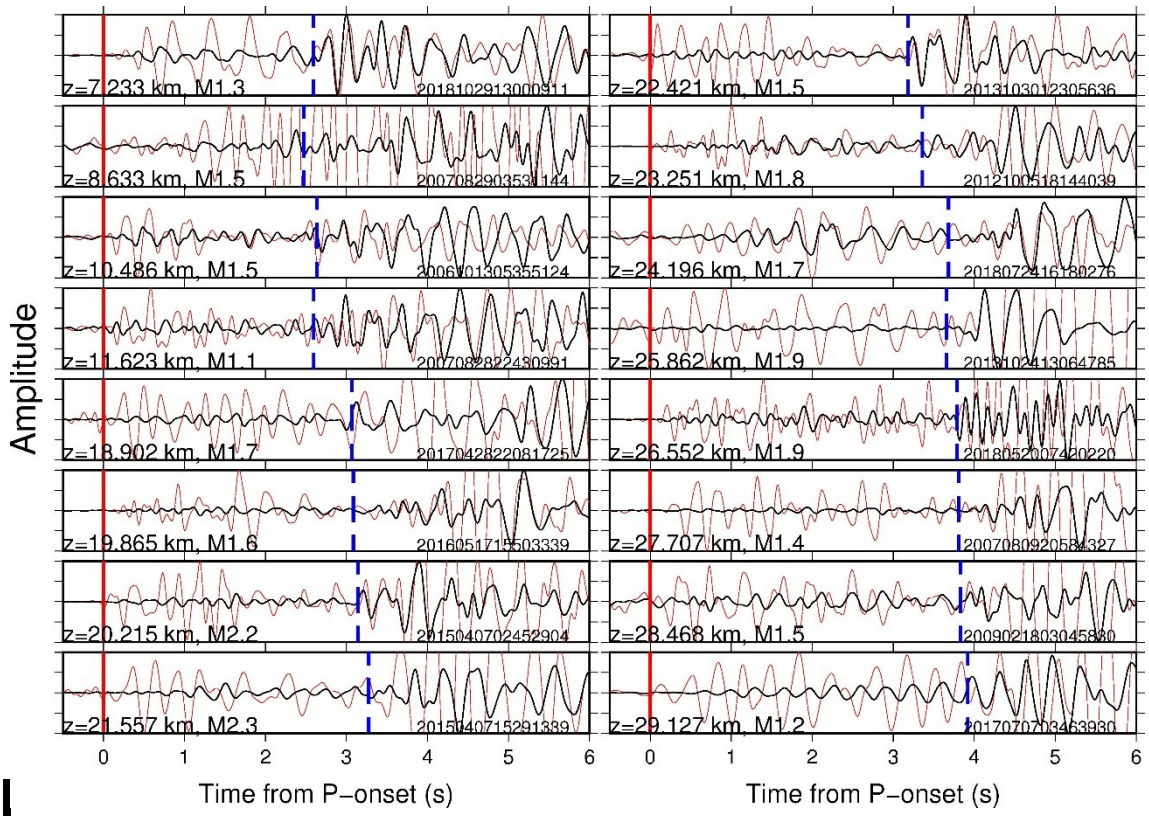

Figure 4. Observed LFE waveforms at a nearby seismic station (HU.ESH). These are ordered according to increasing focal depth. Red and black traces show vertical and transverse components, respectively. Red traces are normalized using the maximum amplitude for the initial 2 seconds from the onset to illustrate P waves. Black traces are normalized using the maximum amplitude for the entire period to illustrate S waves. Blue vertical dashed lines show predicted onset times of S waves according to the relocated hypocentres. The bottom left corner of each trace shows the relocated focal depth (Z) and magnitude (M).

35

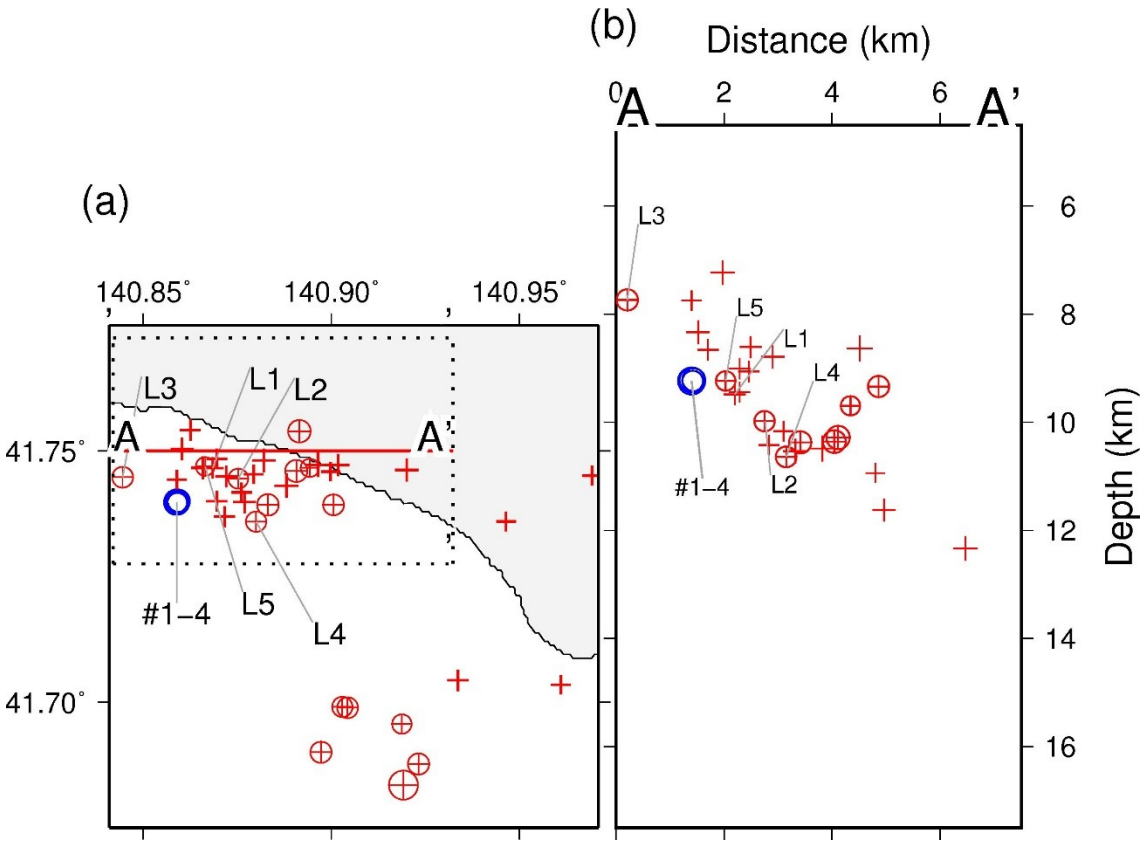

Figure 5. Enlarged view of the spatial distribution of hypocentres in the western region of the study area. (a) Map view and (b) cross-sectional view along line A-A' shown in (a). Red crosses and blue circles show the hypocentres of LFEs and regular earthquakes, respectively, according to the JMA unified catalogue. Red crosses outlined by red circles show events which are classified as regular earthquakes in the JMA unified catalogue but as LFEs in our reclassification.

36

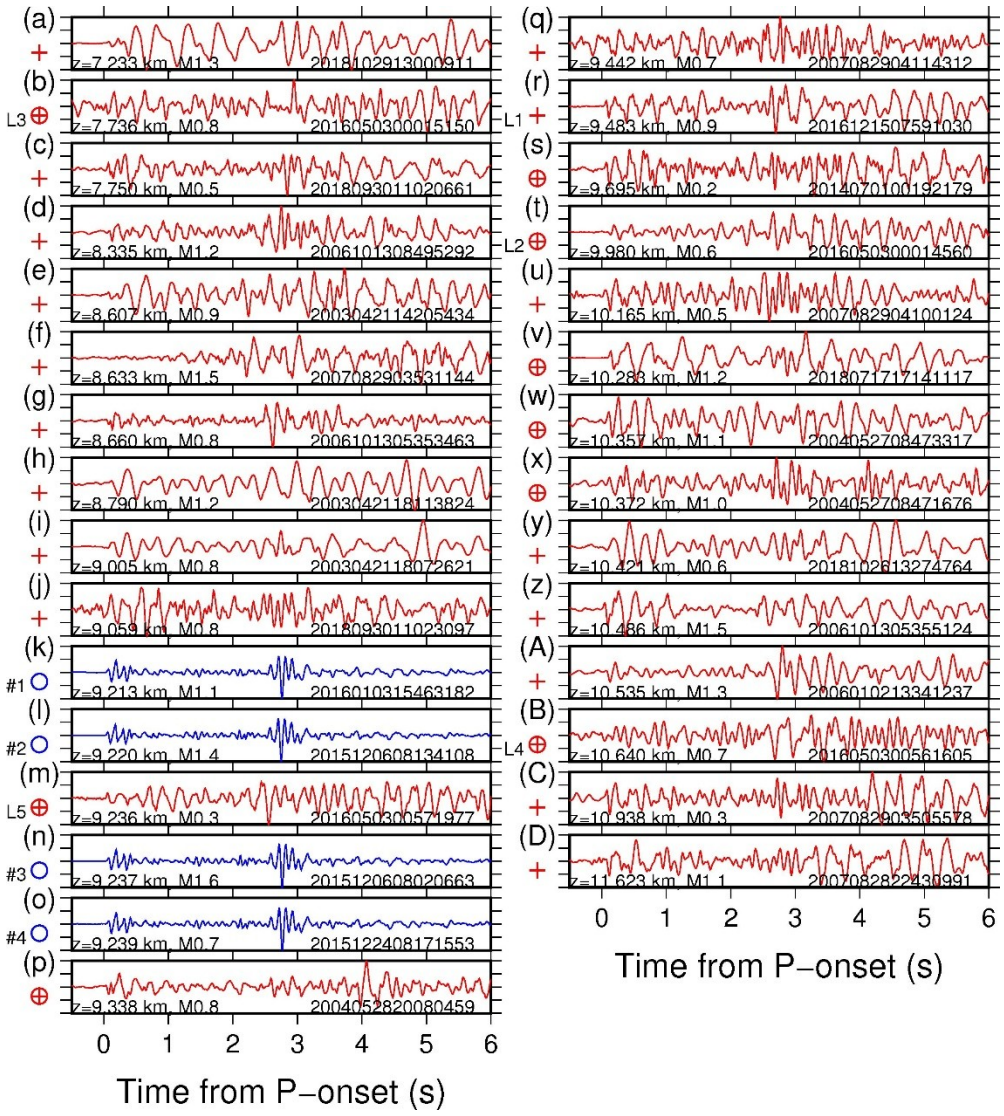

Figure 6. Observed raw waveforms for earthquakes in the western region of the study area obtained at HU.ESH, ordered with increasing focal depth. Red and blue traces show the waveforms of LFEs and regular earthquakes, respectively, according to our classification. Red crosses and blue circles on the left side show LFEs and regular earthquakes, respectively, according to the JMA unified catalogue. Red crosses outlined by red circles show events which

37

732 are classified as regular earthquakes in the JMA unified catalogue but as LFEs in our
733 reclassification.
734

38

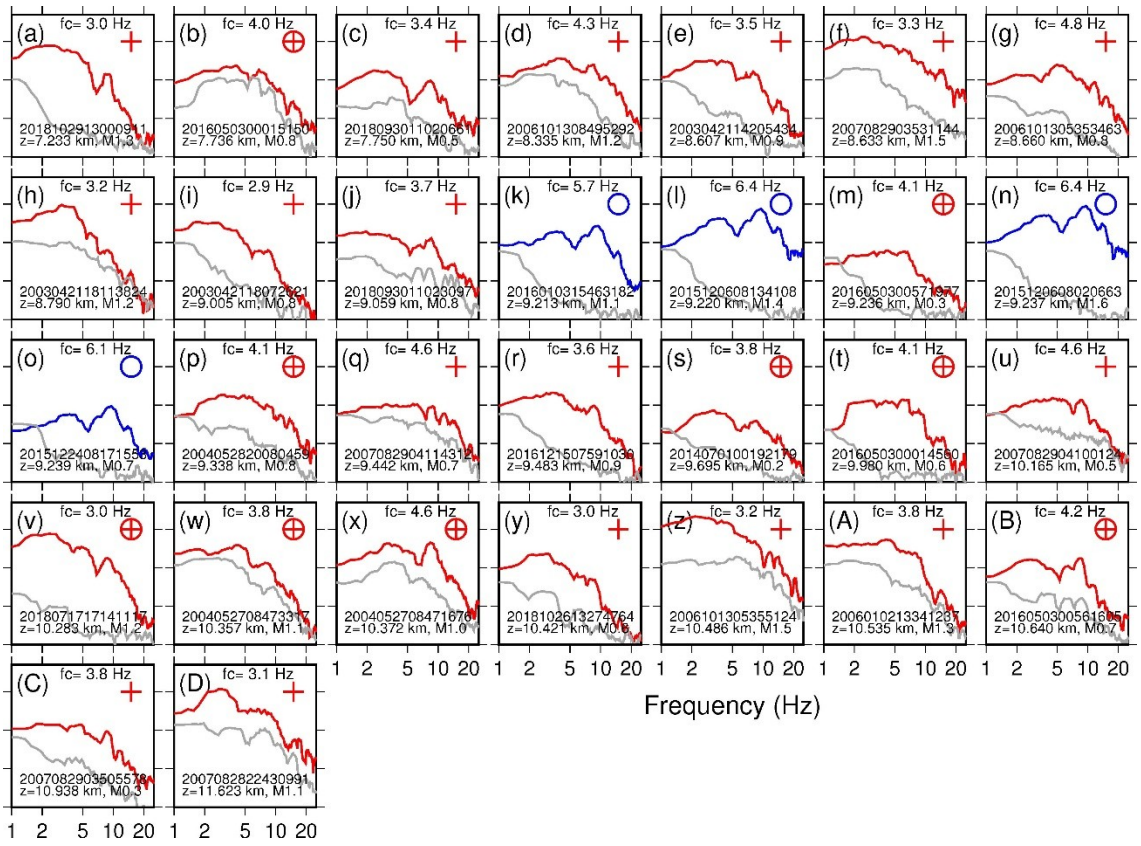

Figure 7. Velocity spectra obtained at HU.ESH for earthquakes in the western region of the study area, ordered with increasing focal depth. Red and blue traces show S wave spectra of LFEs and regular earthquakes, respectively, according to our reclassification. Gray traces show noise spectra. Red cross and blue circle in up-right in each panel shows LFE and regular earthquake, respectively, according to the JMA unified catalogue. Red crosses outlined by red circle show events which are classified as regular earthquakes in the JMA unified catalogue but as LFEs in our reclassification.

39

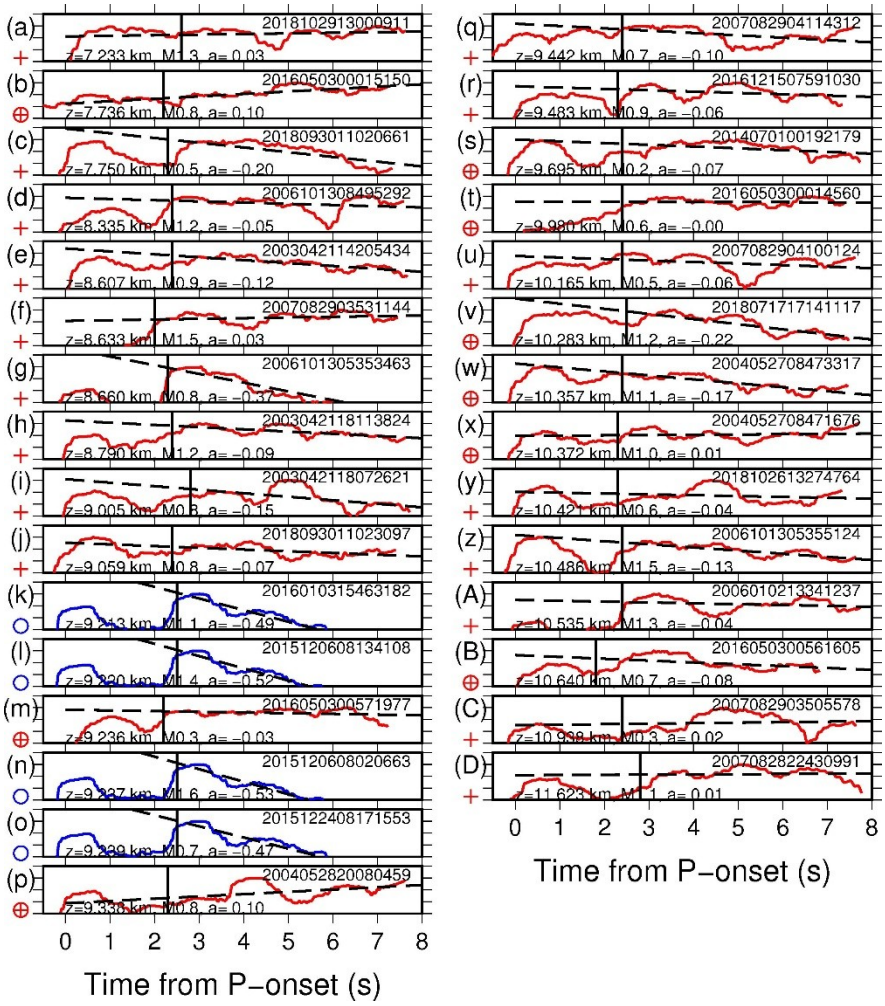

Figure 8. Log waveform envelopes (2–8 Hz) obtained at HU.ESH for earthquakes in the western region of the study area, ordered with increasing focal depth. Red and blue traces show the envelopes of LFEs and regular earthquakes, respectively, according to our reclassification. Vertical lines indicate the arrivals of S wave. Broken lines indicate the lines fitted to the amplitude envelopes after the S wave arrivals. Red crosses and blue circles on the left side show LFEs and regular earthquakes, respectively, according to the JMA unified catalogue. Red crosses outlined by red circles show events which are classified as regular earthquake in the JMA unified catalogue but as LFEs in our reclassification.

40

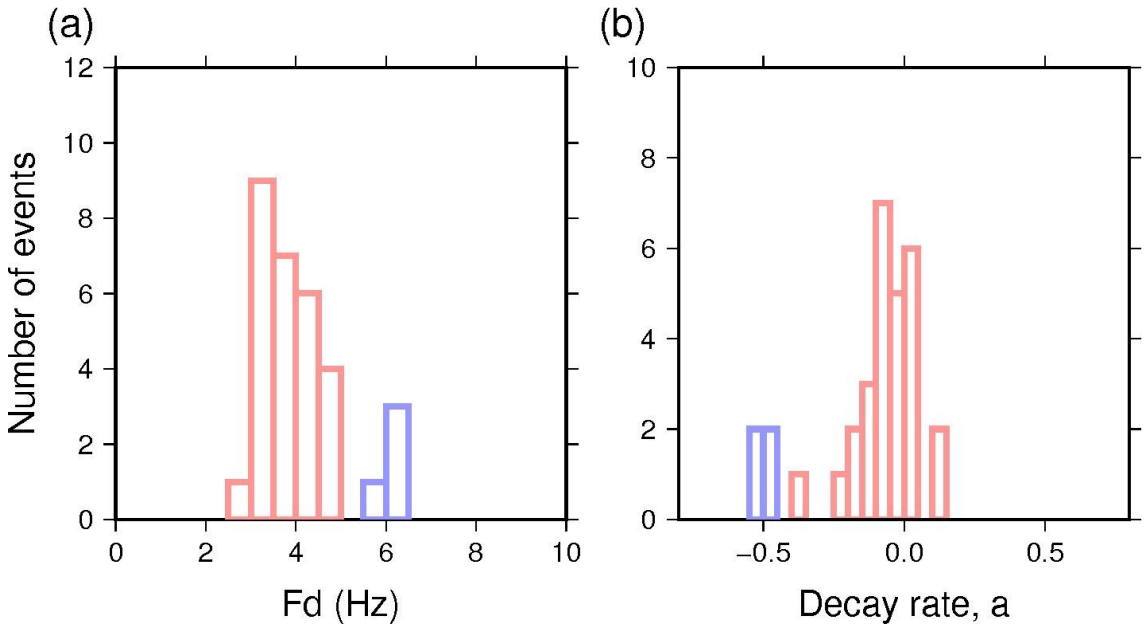

Figure 9. Frequency distributions of (a) dominant frequency and (b) decay rate of amplitude envelope for earthquakes in the western region of the study area obtained at HU.ESH. Red and blue ones show the results of LFEs and regular earthquakes, respectively.

41

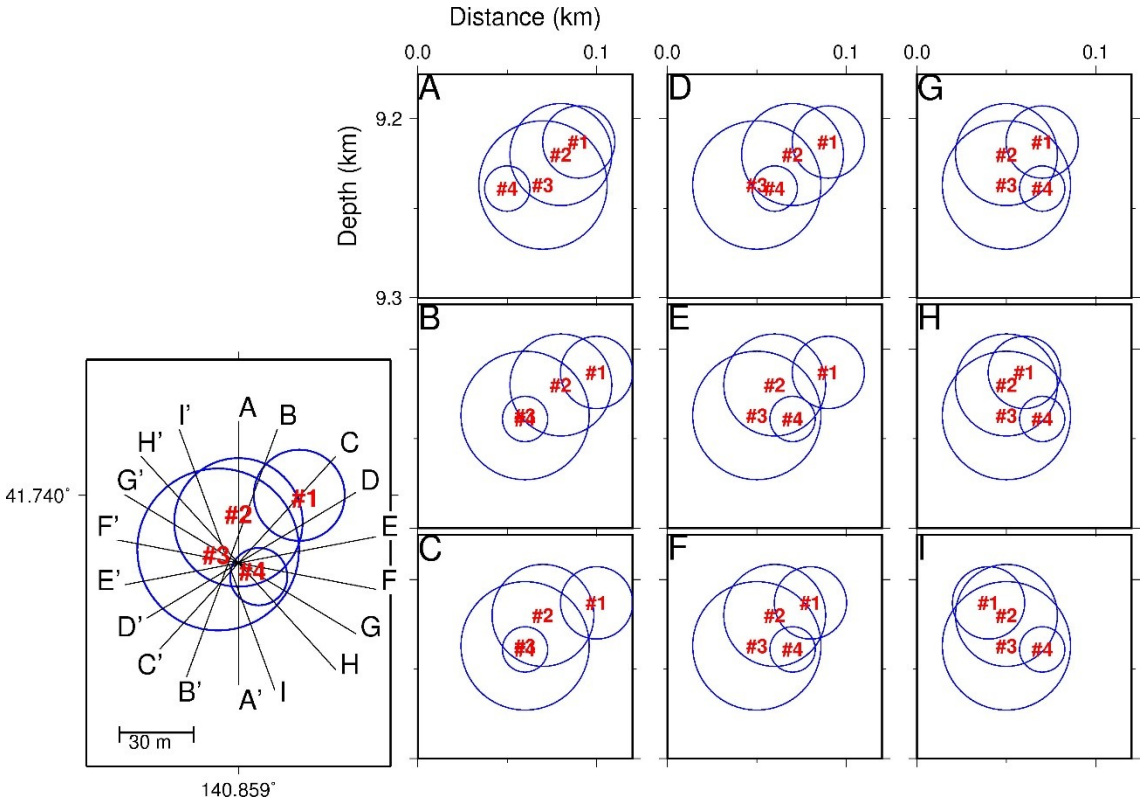

Fig. 10. Map view (left) and cross-sectional views (A–I) of hypocentres of the four regular earthquakes (#1 through #4) in the study area. Size of the circles in the figure corresponds to fault size with a stress drop of 3 MPa, according to Eshelby (1957).

42

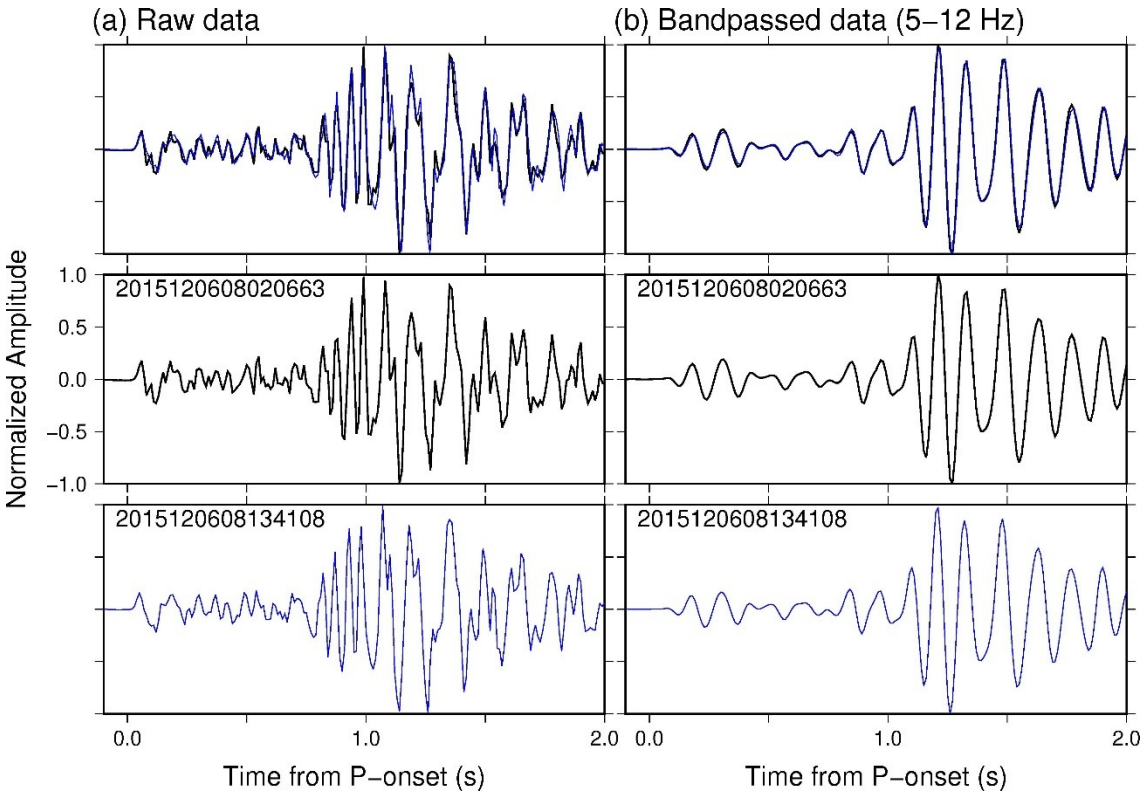

Fig. 11. Observed waveforms (vertical component) for the two largest regular earthquakes at the nearest seismic station (A.TSRN). Their amplitudes were normalized. (a) Raw waveform data. (b) Bandpass-filtered (5–12 Hz) waveform data. The upper figures show the superimposed waveforms of the two earthquakes. Black and blue traces show the waveforms of the largest (M 1.6) and the second largest (M 1.4) earthquakes, respectively. The middle figures show the waveforms of the largest event. The lower figures show the waveforms of the second largest event.

43

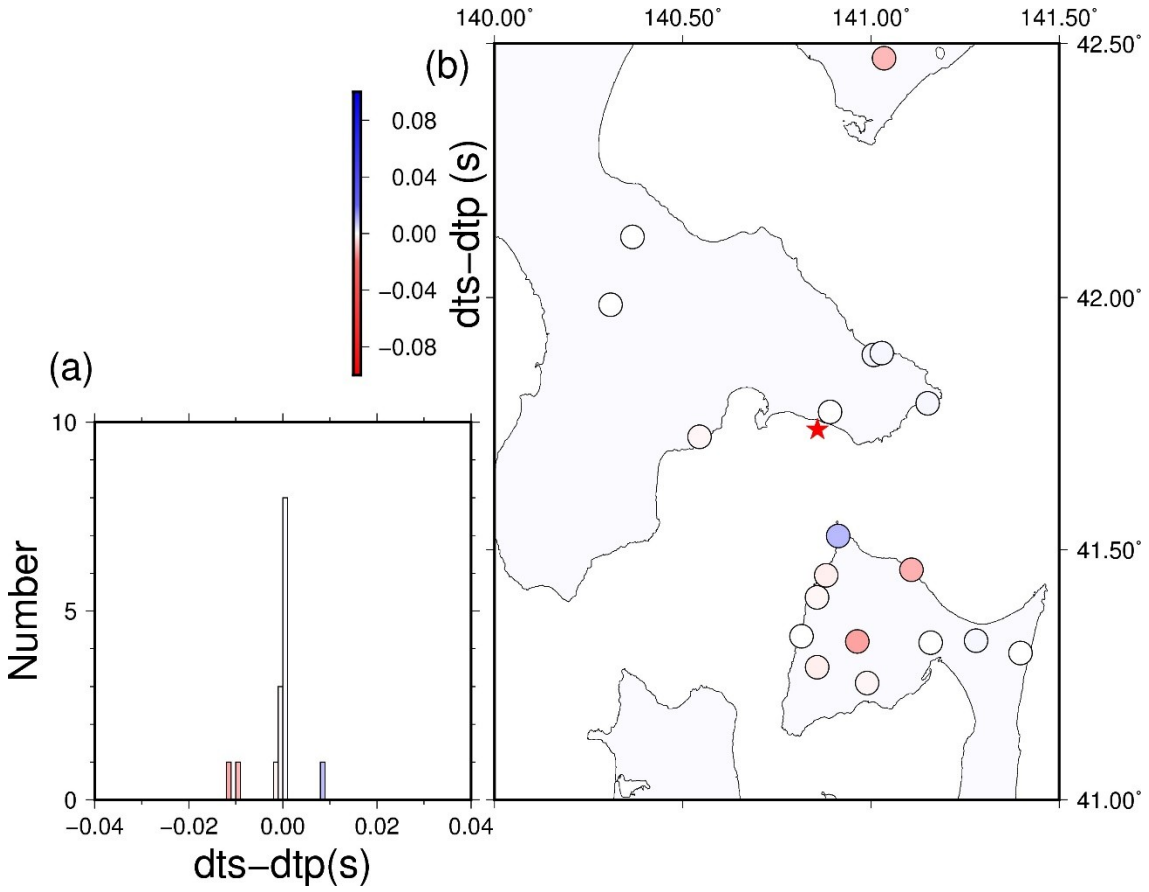

Figure 12. (a) Frequency distribution of the differences in S-P time between the largest event and the second largest event, i.e. the difference of differential arrival times of P ($\mathbf{dt_p}\,\mathbf{dt_p}$) and S waves ($\mathbf{dt_s}\,\mathbf{dt_s}$) at each station. (b) Spatial distribution of $\mathbf{dt_s - dt_p}\,\mathbf{dt_s - dt_p}$ shown at each station location by the colour scale. The star indicates the locations of the two earthquakes.

44

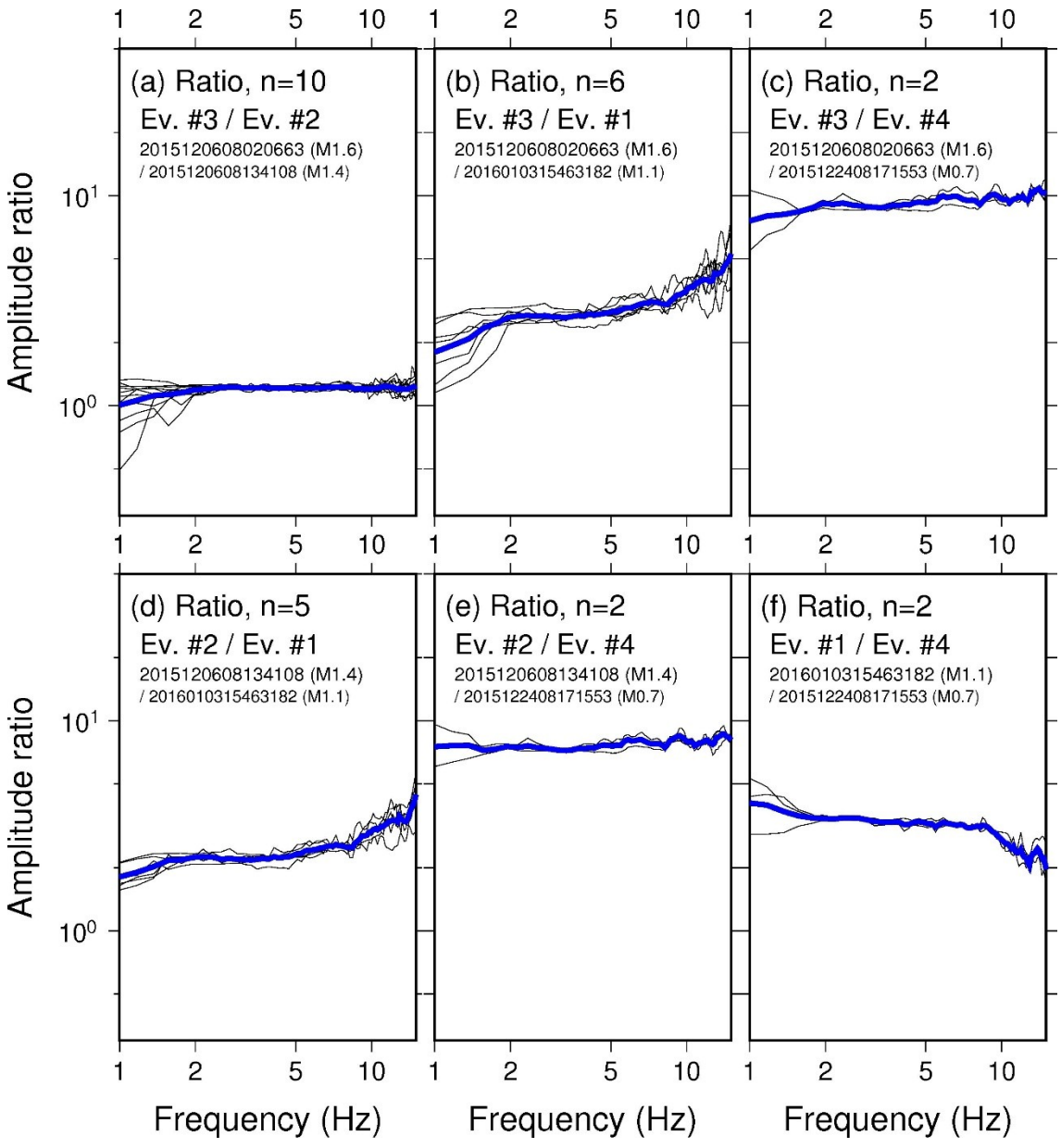

Fig. 13. Spectral ratios of the six combinations of the four regular earthquakes. Black: spectral ratio for each station. Blue: Mean spectral ratio.

45

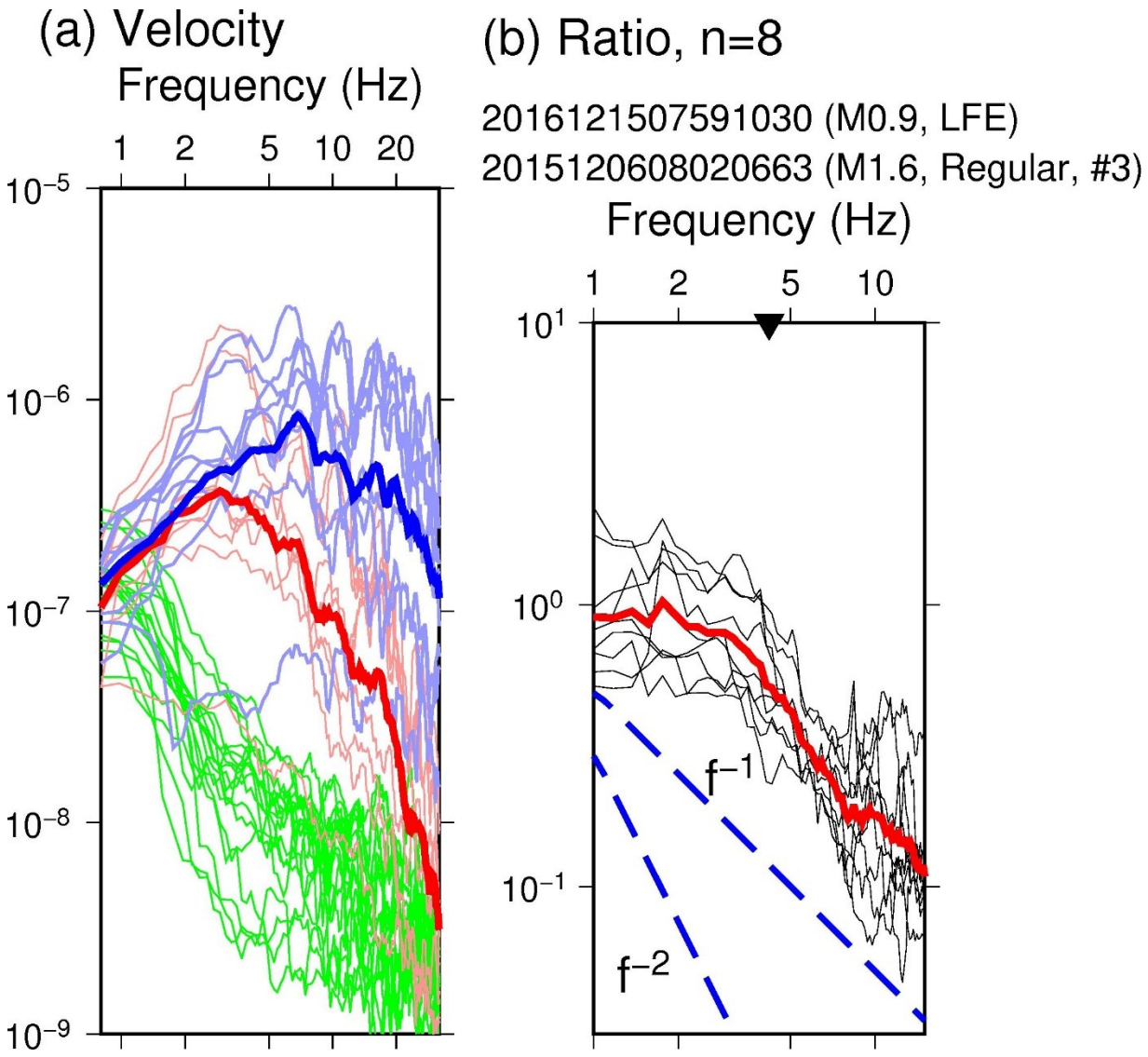

Figure 14. (a) Velocity spectra of an LFE (L1) and the M1.6 regular earthquake (#3). Blue and red curves show the velocity spectra of the regular earthquake and the LFE, respectively, at various seismic stations. Green curves show the noise spectra. Bold curves show the mean spectra. (b) Spectral ratio of the LFE and the M1.6 regular earthquake. The red curve indicates the mean value. Inverted triangle indicates the corner frequency.

46

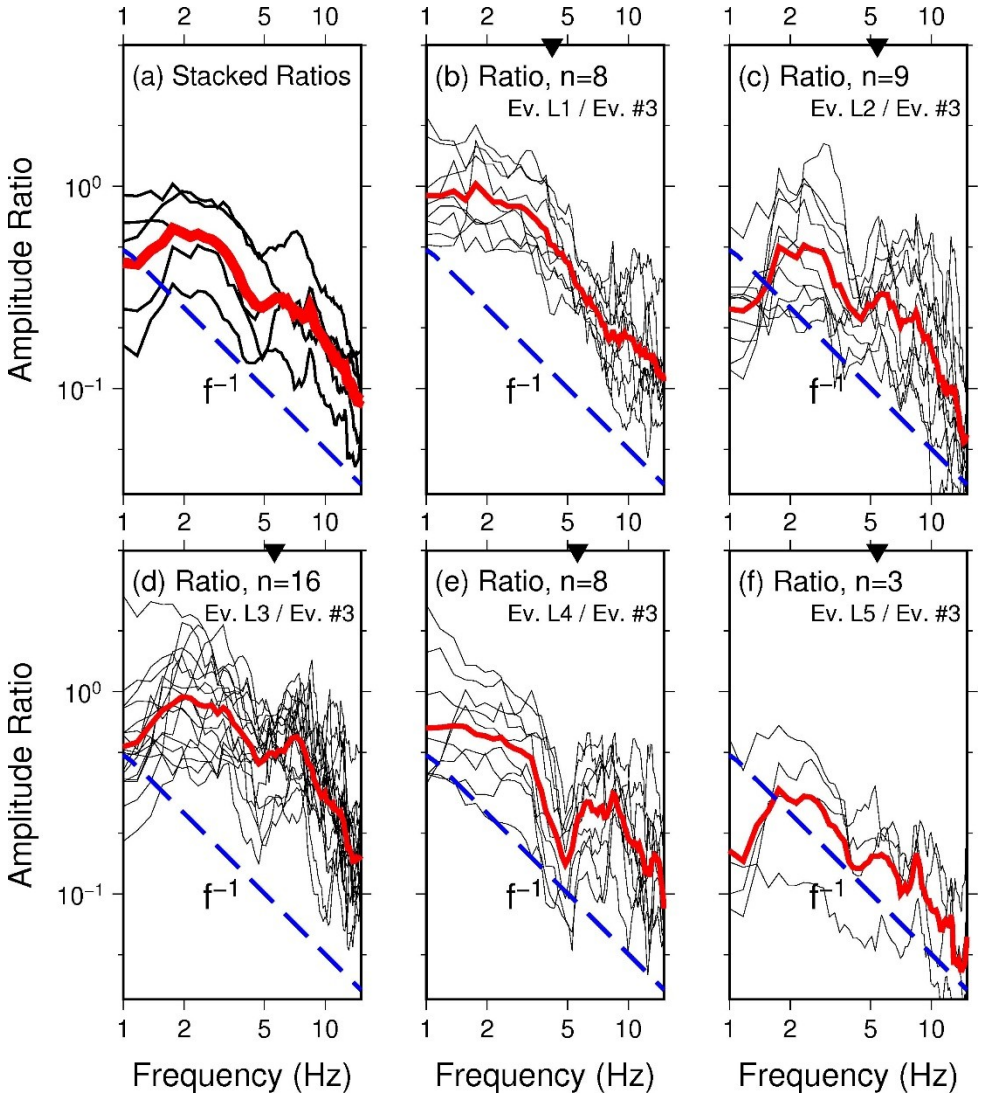

Fig. 15. Spectral ratios between LFEs and the M1.6 regular earthquake (#3). (a) Mean spectral ratios of five different LFEs with the M1.6 regular earthquake (b–f). Black curves show spectral ratios between the individual LFEs and the M1.6 regular earthquake. The red curve shows the mean value. (b)–(f) Spectral ratios of the five LFEs with the M1.6 regular earthquake. Black curves show individual spectral ratios at each channel, and red curves show the mean values. Inverted triangle indicates the corner frequency.

47

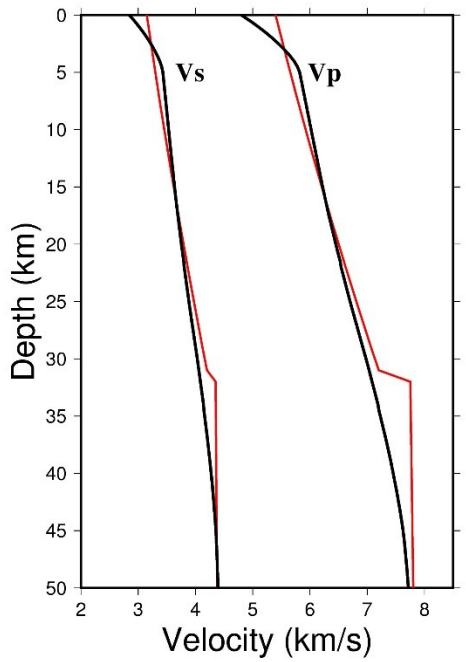

Fig. S1. P and S wave velocity models of Hasegawa *et al.* (1978) (red) and Ueno *et al.* (2002) (black).

48

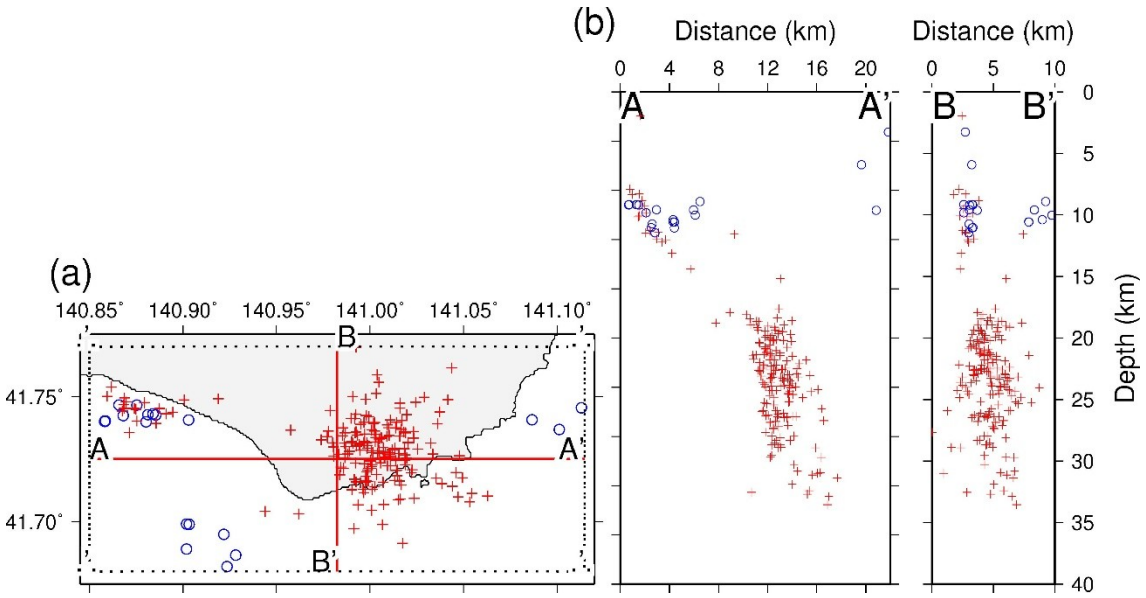

Fig. S2. Relocated hypocentres of regular earthquakes and LFEs in Hakodate, Hokkaido, based on the velocity model of Ueno *et al.* (2002). (a) Map view. (b) Cross-sectional views along lines A-A' and B-B' in (a). Blue circles and red crosses show hypocentres of regular earthquakes and LFEs, respectively.

49

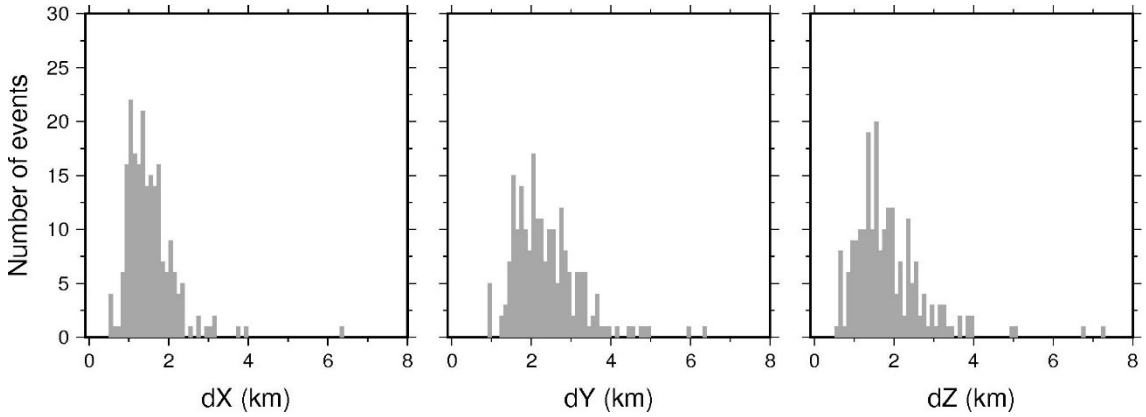

Fig. S3. Frequency distributions of the 95% interval of relocated hypocenters of (a) E–W, (b) N–S, (c) U–D directions.

50

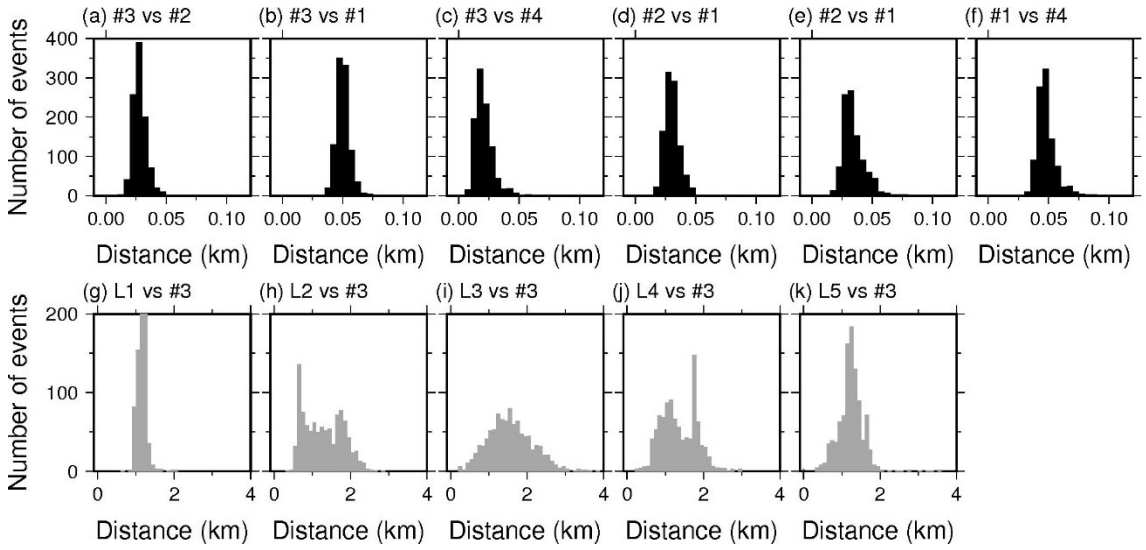

Fig. S4. Frequency distributions of distances of 11 earthquake-pairs in the 95% confidence region according to the 1000 bootstrap results.

51